1

Statistical Thermodynamics of Amphiphile Self-Assembly: Structure and Phase Transitions in Micellar Solutions

Avinoam Ben-Shaul[1]
William M. Gelbart[2]

1.1 Introduction

The main purpose of this chapter is to present a comprehensive, statistical-thermodynamic framework for treating the sizes and shapes of micellar aggregates in aqueous surfactant solutions. In this first section, after a brief historical perspective on experimental studies and theoretical pictures of micellar structure, surface roughness and other fluctuation effects are discussed in the context of both phenomenological and computer simulation studies. In Sec. 1.2 we present the basic self-assembly theory for dilute systems; the aim is to proceed systematically from a formulation of overall partition functions for the aqueous surfactant solution to a phenomenological discussion of effective chemical potentials. By deriving this latter language, we make contact with the highly useful "law of mass action" approach which has been pursued by most workers in their analyses of micellization and size/shape effects in dilute solution. We also feature there the role of "dimensionality of growth", i.e., the basic differences between the concentration dependence of equilibrium sizes in the case of sphere ("zero-dimensional"= 0D)-, rod (1D)-, and disk (2D)-like aggregates. Following a brief discussion of the structures and relative stabilities of vesicles and mixed micelles, we close Sec. 1.2 with some remarks on the much-neglected

[1]Department of Physical Chemistry and The Fritz Haber Research Center for Molecular Dynamics, The Hebrew University, Jerusalem 91904, Israel
[2]Department of Chemistry and Biochemistry, The University of California, Los Angeles, California 90024, USA

and highly problematic question of "rotation/translation" contributions to micellar partition functions (and hence to the effective surfactant chemical potentials).

Section 1.3 treats the problem of separating the effects of amphiphilic "heads" and "tails" in statistical thermodynamic descriptions of micellar aggregates. The prevailing ideas concerning predictions of preferred shapes are discussed critically. We also outline there the nature of chain packing in micelles and the contribution of chain degrees of freedom to the free energies of surfactant molecules in aggregates of different curvature; in this context, a microscopic basis is provided for the bending elasticities of amphiphilic mono- and bi-layers. In Sec. 1.4 we introduce the reader to recently developed ideas concerning the way in which interactions between micelles can lead first to the enhancement of size in isotropic solutions and then to the onset of orientational and positional long-range order in nematic, hexagonal and lamellar states of concentrated surfactant-water systems.

The concept of a *micelle* as an aggregate of surfactant molecules arose in the early part of this century when McBain [1] in 1913 first sought to understand the anomalous concentration dependence of many physical properties of aqueous soap solutions. In the words of Debye [2]: "Soap solutions exhibit even lower osmotic activity than would be predicted if one assumed that soap existed in solution as simple undissociated molecules. They also conduct the electric current far better than would be expected from the observed osmotic effects." Figure 1.1 represents these effects and correlates their breaks in slope with sudden rise of turbidity and with leveling off in surface tension reduction, i.e., with onset of micelle formation in bulk solution. To continue in the words of Debye, writing in 1949: "Since 1913, investigators have shown considerable interest in the determination of the size and shape of the micelle." As an introduction to the subject of this chapter, in fact, it is useful to proceed further with a look at the work of Debye.

The experiments which Debye reported in his 1949 paper [2] involved light scattering studies of a series of n-alkyl trimethyl ammonium bromides [$C_nH_{2n+1}N(CH_3)_3^+Br^-$]. From the plots of turbidity (τ) vs. surfactant concentration (c) it was concluded that, above a *critical micelle concentration* (CMC) aggregates appear as the dominant species: "The curves resemble typical τ vs. c plots for polymer solutions." For these latter systems Debye had already shown that a plot of turbidity vs. concentration would yield the molecular weight M as its slope at the origin ($c \rightarrow 0$). Hence the "Debye equation" for molecular weights of micellar aggregates [3]

$$\frac{K(c - CMC)}{\tau} = \frac{1}{M} + 2A_2(c - CMC) \tag{1.1}$$

where K is the "optical" constant (determined by the incident wavelength

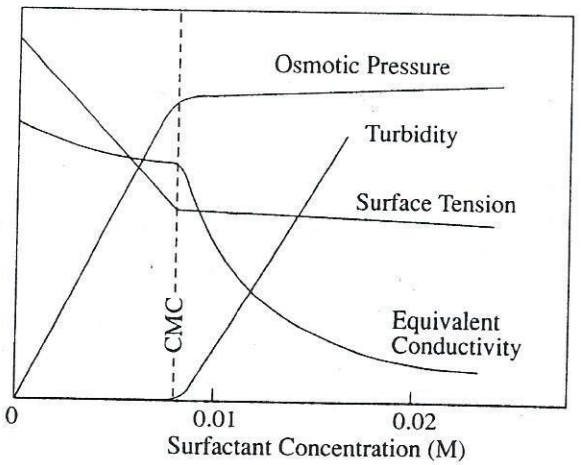

FIGURE 1.1. Effect of micellization on bulk properties of surfactant solutions. Note, for example, that the osmotic pressure is proportional to the total concentration of *particles* (monomers plus micelles). Above the CMC the added surfactants form micelles, and the increase in total particle concentration is small. On the other hand, the turbidity is proportional to the concentration of micelles. The CMC value and the concentration scale correspond to an aqueous solution of SDS (sodium dodecyl sulfate) (after Refs. 3 and 33).

and indices of refraction of the solvent and solution) and A_2 is the second (osmotic pressure) virial coefficient. Figure 1.2, reproduced from the original work of Debye [2], shows the first light scattering estimates of micellar size. "The heights of the vertical lines drawn at the critical concentration represent the reciprocal molecular weights of the micelles" [2]. Note how micellar size increases with carbon number.

Debye also suggested an additional technique for determining micellar size. He observed in particular that "in the presence of relatively high salt concentrations the micelles of the longer-chain detergents are large enough to cause measurable disymmetry in the intensity of the scattered light" [4]. On the basis of such measurements (on n-hexadecyl trimethyl ammonium bromide in 0.2M KBr) it was concluded that the micelles underwent a transition from spherical to rod-like aggregates upon increase in surfactant concentration above the CMC. This idea has been refined and pursued vigorously by many workers during the past thirty-five years. Ikeda *et al.* [5], for example, have measured the angle dependence of the

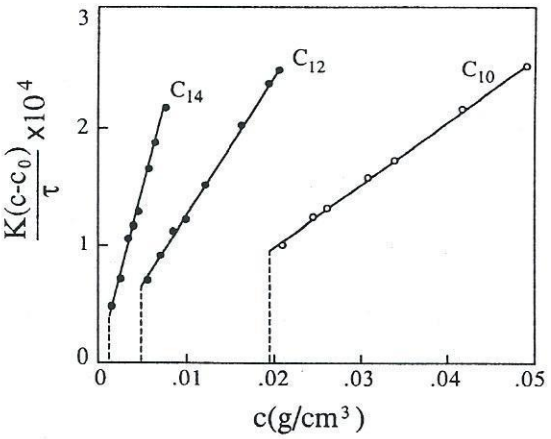

FIGURE 1.2. Reciprocal specific turbidities vs. surfactant concentration for solutions of n-alkyl trimethyl/ammonium bromides in water [2].

turbidity as a function of surfactant concentration in high-salt (0.8M NaCl) aqueous solutions of dilute sodium dodecyl sulfate (SDS). Figure 1.3 shows some of their results for $T = 35°C$. The intercept of each curve gives the reciprocal weight-average molecular weight (assuming $A_2 = 0$ in (1.1)), and the slope gives the radius of gyration. Thus, for the high concentration curve, $c = 1.10 \times 10^{-2}$g/cm^3 ($\approx$ 100 CMC), one finds an aggregation number of $\approx$ 1000 molecules/micelle (about six times the size at the CMC). The average micellar length, if the micelles are rod-like, is found to be $\approx$ 600Å, as compared to their diameter which is estimated to be $\approx$ 40Å. Better estimates of the size can be obtained by fitting the data to (1.1) with A_2 calculated assuming that the micelles are rigid rods [5].

An entirely independent technique for determining the size of micelles involves *dynamic* light scattering in which the homodyne autocorrelation function [6] of the quasielastic intensity is measured. Application of this approach to surfactant solutions was developed primarily by Benedek and coworkers [7] in the U.S. and by Corti and Degiorgio [8] in Italy. Approximately what one does is extract the mean translational diffusion coefficient D from the autocorrelated intensity and then use the Stokes-Einstein relation to infer the hydrodynamic radius $R_H = kT/6\pi\eta D$, where k is Boltzmann's constant and η is the solvent viscosity. (See Sec. 2.2.1 for further discussion of this light scattering approach.) In practice the spread in micellar sizes leads to a nonexponential homodyne signal, and a cumulant analysis is necessary to deduce the first several moments (and hence the average, variance, skewness) of the distribution.

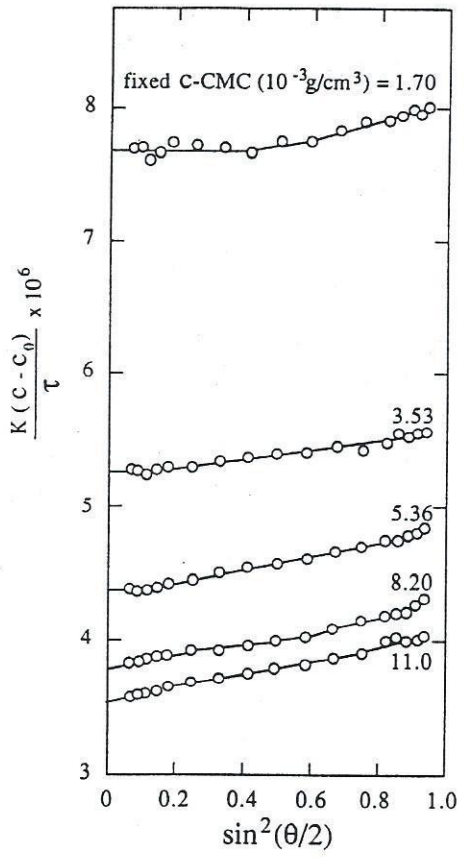

FIGURE 1.3. Angle dependence of light scattering intensity from sodium dodecyl sulfate solutions in 0.80M NaCl at 35°C [5].

Another complication arises because the measured diffusion constant contains contributions from the interactions between micelles. More explicitly, D varies with concentration c according to

$$D = D_0(1 + k_D c) \tag{1.2}$$

where k_D is a simple functional of the inter-aggregate potential [9]. A similar relation holds for the "apparent" ("intrinsic", i.e., single-micelle) molecular-weights which contribute to the *static* intensity—see (1.1). It follows that the increase of M and R_H with concentration need not imply a growth of micelles, but rather "only" the effect of interactions. The relative importance of the two effects depends on the composition (i.e., surfactant, added salt, etc.) and temperature of the solution in question.

In the late 1970's and early 1980's there was considerable controversy surrounding the interpretation of several quasielastic light scattering studies of micellar size in ionic amphiphilic systems—see [5,7] and the more recent overviews given by these same workers [10]. It is now agreed that a high concentration of added salt is necessary to suppress (screen) the interaggregate (electrostatic) potential contributions to the diffusion coefficient; only at large ionic strength can one deduce safely that the mean micellar size is truly increasing with surfactant concentration. We note that polydispersity and interaction contributions complicate similarly the inference of micellar size from viscosity [11] and dynamic Kerr (electric field-induced birefringence) [12] measurements.

Valuable information about the structure of micelles in dilute solution is also provided by small-angle neutron scattering data [13]. In these experiments one is probing heterogeneities on length scales d of order $10-1000\text{Å}$, corresponding to scattering vectors with magnitudes $q = 2\pi/d$ in the range 0.006 to 0.6Å^{-1}. At this spatial resolution the different micellar regions and the solvent can be regarded as continuous media, with the scattering amplitude for the n^{th} aggregate given by

$$A_n(q) = \int_{V_n} dr e^{i\mathbf{q}\cdot\mathbf{r}}[\rho_n(\mathbf{r}) - \rho_s]. \tag{1.3}$$

Here $[\rho_n(\mathbf{r}) - \rho_s] \propto [\sum_{i\varepsilon n} b_i \delta(\mathbf{r} - \mathbf{r}_i) - \rho_s]$ is the excess (with respect to solvent's) density of scattering length in the n^{th} micelle, b_i being the nuclear scattering length for the i^{th} nucleus in n (located at $\mathbf{r}_i$) [13] and V_n is the nth aggregate's volume. The static ("elastic") intensity measures the thermal average of the square of this amplitude, after it has been summed (with appropriate phase factors) over all aggregates:

$$I(q) \propto \left\langle |A(q)|^2 \right\rangle \tag{1.4}$$

with

$$A(q) = \sum_{n=1}^{N} A_n(q) e^{i\mathbf{q}\cdot\mathbf{R}_n} \tag{1.5}$$

where $\mathbf{R}_n$ is the center of mass position of the n^{th} aggregate, and $\langle\cdots\rangle$ denotes the thermal average of $\cdots$.

For globular micelles, weak correlations between the positions of aggregates and their orientations and sizes allow the scattering cross section to be approximated by [14]

$$I(q) \propto \left[\left\langle |A_1(q)|^2 \right\rangle + \langle A_1(q)\rangle^2 \left(S(q) - 1\right)\right]. \tag{1.6}$$

Here, $S(q)$ is the usual *structure factor* describing the interferences between the centers of mass of different micelles, i.e., the Fourier transform of the pair correlation function. $\langle A_1(q)\rangle$, the single particle *form factor*, is the Fourier transform of the *average* distribution $\rho(\mathbf{r}) - \rho_s$ of excess

scattering length within an aggregate, the brackets denoting specifically an average over all sizes. Similarly, $\langle |A_1(q)|^2 \rangle$ is the transform of the average "Patterson function" $\int d\mathbf{r}[\rho(\mathbf{r}) - \rho_s][\rho(\mathbf{r}+\mathbf{R}) - \rho_s]$ for an aggregate [15], containing therefore the effects of nonspherical shape and size polydispersity. Note then that, even in the absence of interparticle interferences (i.e., for situations where only the first term in (1.6) is important) the interpretation of $I(q)$ is problematic. Hayter [16] has shown, for example, that for any solution of *monodisperse ellipsoids* there corresponds a *polydisperse sphere* system which leads to the same form of $\langle |A_1(q)|^2 \rangle$. At higher concentrations, where $S(q) \neq 1$, it becomes only more difficult to infer the micellar sizes and shapes.

Cabane *et al.* [17] have emphasized the importance of large q measurements for determining the fluctuations in micellar size and shape. They argue in particular that for scattering data extending out only to some maximum wavenumber q_m, details in structure corresponding to distances smaller than π/q_m will not be resolved. Using "contrast variation tricks", however, it is possible to measure separately the average radius (R_c) of the hydrocarbon core of a micelle and that (R_p) of the *whole* aggregate (core plus layer). "Contrast" between density profiles is achieved via H/D isotopic substitution which shifts the scattering lengths (b) of methylenes from -0.083 (CH_2) to $+1.999$ (CD_2) and of methyls from -0.457 (CH_3) to $+2.666$ (CD_3); similarly, for $H_2O \rightarrow D_2O, b = -0.168 \rightarrow +1.92$. It is thus possible to "label" a surfactant molecule in many different ways (e.g., degrees of alkyl deuteration); then, by using alternately H_2O or D_2O as a solvent, one can generate several micellar solutions and hence as many relations between the number densities $n_i(r)$ of methyls, methylenes, polar heads, and counterions in and around the micelle of a given proposed structure. More explicitly, one models the density averaged scattering length distribution $\rho(r)$ as a linear combination of nuclear scattering lengths b_i : $\rho(r) = n_1(r)b_1 + n_2(r)b_2 + \ldots$. Then selective deuteration ("contrast") provides the required number of linear relations for determining the spatial distribution of the various functional groups (e.g., methyl, methylene, etc.) in the aggregate. This procedure requires, of course, that such isotopic substitutions do not disturb the micellar structure [18].

In virtually all cases, the elastic neutron scattering techniques described above have been restricted to studies of essentially *globular* (i.e., approximately spherical) micelles [19]. Small q data have been exploited to obtain much information about the average structural features of these surfactant solutions, such as the average aggregation number N and the average charge Z of a micelle. In extracting such information, the structure factor, $S(q)$ in (1.6), has been estimated from approximate analytical theories of interferences between charged hard spheres in water [20]. Since differences between $\langle |A_1(q)|^2 \rangle$ and $\langle A_1(q) \rangle^2$ are small at low q, the micellar model is defined crudely by only two parameters, N and Z, i.e., fluctuation effects involving size/shape and charge are suppressed. $\langle A_1(q) \rangle^2$ and

$S(q)$—and hence $I(q)$— are calculated for each choice of average values, N and Z, and correlated iteratively via successive comparisons between computed and observed (low q) scattering distributions. As already stressed above, *large* q data are required to deduce meaningful information about *fluctuations* from the average micelle. Many workers have discussed how these latter experiments, as well as $q \to 0$ "contrast variation" studies, can provide details on the nature of size and shape distributions for globular ("almost spherical") aggregates and of the structures of interfacial regions and the conformational statistics of alkyl chains in these micelles. Again, however, scattering analyses of this kind are no longer possible in the case of anisotropic and polydisperse (e.g., long rod-like) aggregates at higher concentrations (see Chap. 2).

At high amphiphile concentrations the aggregates organize into positionally ordered phases. In this chapter we focus our interest on *finite* rod-like micelles in *positionally disordered* solutions, but also comment briefly on their evolution in columnar phases (see Sec. 1.4.3). To complement our present introduction, we remark as well on the classic (i.e., essentially infinite aggregate) lamellar and hexagonal phases of surfactant/water systems. (The lamellar states are treated comprehensively in Chaps. 4, 5 and 6.) Here, the basic structural determinations were provided more than thirty years ago by Luzzati, Mustacchi, Husson and Skoulios [21]. They used X-rays to measure organizational changes in solutions of fatty acids in water as a function of temperature and concentration, the Bragg diffraction pattern for each long-range translationally ordered phase being analyzed in terms of its characteristic reflection indices [22]. For uniformly spaced reflections $(1/d, 2/d, \ldots \text{Å}^{-1})$, for example, the aggregation state corresponds to stacked *bilayers* (lamellae) with spacing (one-dimensional lattice constant) d. Knowing d and the overall volume fraction of amphiphile in water one can deduce the lamellar thickness D. The sharp Bragg reflections typically observed in these systems provide direct evidence for the minor role played by fluctuations in the lamellar phase. In other words, bilayer packing of the surfactant molecules is the overwhelmingly preferred curvature mode under high concentration (and/or high salt, added alcohol) conditions. (See, however, the discussion of fluctuation effects in Chaps. 5 and 6.) Similarly, the interaxis spacing d' and diameter D' corresponding to *cylindrical* aggregates in *hexagonal* states can be inferred for each of these soap systems at higher water content. A typical result is shown in Fig. 1.4. Considerable experimental [23,24] and theoretical [25] work has been done recently to further document and explain data of this kind. But many unanswered questions remain concerning the nature of defects in those systems [26–28], the mechanism of their phase transition [26,27], and the microscopic details of the chain packing and head-group organization in them (see Sec. 1.3).

We have already noted that most experimental investigations have been concerned with small globular micelles just above the CMC. Similarly, a considerable theoretical effort has been devoted to describing head-group

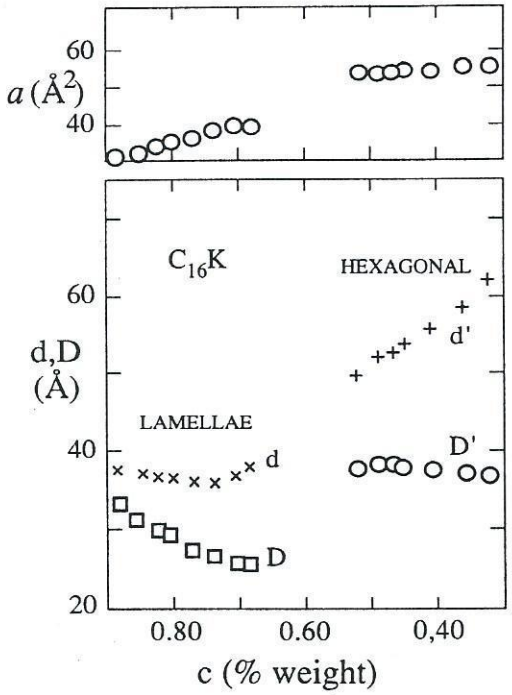

FIGURE 1.4. Distance between sheets (d) and cylinders (d') and their thicknesses (D and D') in lamellar and hexagonal phases of $CH_3-(C_2)_14COO^-K^+$ (palmitic acid salt), as a function of concentration. These data can be used to calculate the area, a, per surfactant head-group in each of the two phases as a function of concentration, as shown in the upper panel [21d].

organization in the interfacial region, and "tail" conformations in the hydrophobic core, of these "minimum" ("almost spherical") aggregates. Gruen [29] has presented a critical synopsis of the available experimental findings. His analysis supports the "standard" picture according to which [30–33]:

- on average, almost all of the hydrocarbon chain of each amphiphile lies within the micellar core.
- hydrophilic species (i.e., head-groups and aqueous solution) are nearly completely excluded form the core.
- the amphiphilic (alkyl) tails fill the core at a nearly uniform, approximately liquid n-alkane, density, the semi-flexible chains showing a high degree of conformational disorder.

In essence, this approach asserts that a useful, first-order, picture of micellar structure follows from a division of the amphiphilic volume into *core* and *interfacial* regions, each described by relatively simple geometries. On a more molecular scale, it argues that many basic features of micellar organization (e.g., chain statistics, solubilization properties, etc.) can be accounted for without giving up the notion of a well-defined aggregate. In particular, as we shall see in Sec.1.3 below, the assumption of a dry, liquid-like core with monomer (CH_2 segment) density $\rho_{CH_2} \approx \rho_{CH_2(\text{liquid alkane})}$ can be shown to yield bond orientational order profiles and labeled segment distributions in close agreement with experiment. The probability of a terminal segment (methyl group) sitting at the surface of a spherical micelle, for example, is significant, even though its most probable location is halfway to the center. Indeed, *all* segments have a non-negligible probability of lying at the surface, because most of the volume of a small globular aggregate is associated with its outer shell. It is this simple geometric fact which reconciles a dry hydrophobic core with large interfacial contact between chain segments and water: there is no need to insist on significant penetration by water. (For alternative models of micelle structure, see, e.g., [34,35].)

Recently, several machine simulation attempts have been made to test the above picture of micellar structure. The earliest efforts, Monte Carlo (MC) calculations by Pratt *et al.* [36], do not treat water or ionic surfactants on a truly microscopic level, introducing instead a phenomenological account of short chains on a lattice. Similarly, the molecular dynamics (MD) calculations of Haile and O'Connell [37] do not directly test the nature of equilibrium aggregates, because they essentially *impose* a given shape by constraining the amphiphile head-groups to undergo translations and small amplitude oscillations within a spherical shell. Aqueous solvent does not appear explicitly in their theory. Instead, the hydrophobic effect involving water and methylenes is incorporated by a short-ranged repulsive shell displaced slightly from the head-group sphere. Nevertheless, one can obtain useful information from these sorts of simulations about the segment density distributions and bond conformational statistics. Indeed, by following the molecular dynamics of chains interacting in this geometry via realistic potentials, one generates an essentially exact solution to the problem of constrained surfactants. In this context Haile and O'Connell present a detailed comparison between their results and those obtained in earlier, mean-field theories which also assume a dry spherical core with head-groups confined near the surface. Good agreement is found, for reasons which we shall explain in Sec. 1.3.3, where we treat in some detail the mean-field approach to chain statistics.

In order to address on a microscopic level the still more fundamental questions of micellization, it is necessary to consider machine simulations which do not impose at the outset any particular form for the equilibrium aggregates. Indeed, the micelle must be observed to form sponta-

neously from our having simply put surfactant molecules into water at high enough concentration. First steps in this direction have been taken by Jönsson, Edholm and Teleman [38], and by Watanabe, Ferrario and Klein [39], who studied the formation of sodium octanoate micelles in aqueous solution via molecular dynamics simulations. Here, the water is described by the point-charge effective pair potential which is known to give a good account of bulk liquid water properties. Watanabe *et al.* introduce site-site interactions and conformational energies involving the alkyl chains, and Lennard-Jones combining rules for all atoms and pseudo-atoms (e.g., CH_2, CH_3) as well as charges on the head-group oxygens and carbons and, of course, on the sodium ions. Long range Coulomb interactions between charges are calculated via Ewald summation. (Jönsson *et al.* introduce somewhat different charges, and simply truncate the electrostatic forces beyond 10Å.) Periodic boundary conditions are used with a cubic box having side length 34.2Å containing 15 surfactant molecules ("monomers") and 1068 waters. Note that this situation necessarily implies a mole fraction of over 1%, i.e., a concentration of surfactants that is orders of magnitude larger than the CMC and that is already large enough for ordered phases to form! An investigation of micelles in *dilute* solution would require not only many (i.e., 10^2 times) more water molecules, but also that trajectories be followed for much (i.e., 10^3 times) longer times in order to follow the *spontaneous* appearance of the aggregates. Both improvements are well beyond the power of present molecular dynamics computations. Nevertheless, it is not unlikely that these goals will be achieved in the foreseeable future as indicated by the most recent studies of Smit *et al.* [40]. These authors performed molecular dynamics simulations using a parallel algorithm (employing 100 transputers) on a model system of nearly 40000 particles representing surfactant, water and oil molecules. The model particles are drastically simplified versions of the real molecules, yet the system features many of the essential properties of real surfactant solutions, including spontaneous micellization in the water phase.

The simulation in [39] begins with a micelle of 15 octanoates with head-groups constrained to the surface of a sphere whose radius is chosen to give a core with density equal to the liquid alkane value. After the solvent is prepared by equilibrating 1331 water molecules (corresponding to a pure water density of 1g/cc), the micelle is introduced at the box's center and all overlapping waters removed. Finally, sodium counterions are substituted for an equivalent number (15) of waters chosen randomly on a shell of radius of about 6Å larger than that of the micellar core. The whole system is then equilibrated for 50ps with constrained head-groups, after which time these constraints are released and the full molecular dynamics simulation is begun ($T = 300$K, with a time step of 2.5 fs.). Analysis is done on 250 ps trajectories, with most of the data obtained during the last 50 ps of calculation. Because the simulation cannot be carried out for longer times,

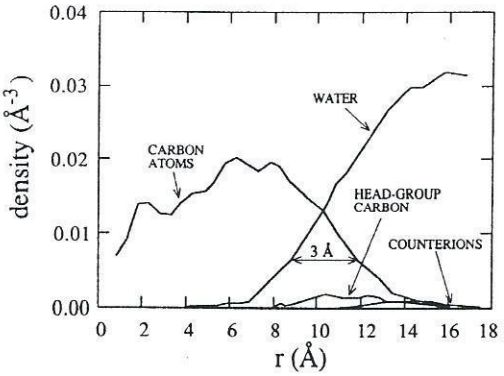

FIGURE 1.5. Density of carbon atoms, water molecules, surfactant head-groups, and counterions, as a function of the distance from the center of the micelle. The results were obtained by molecular dynamics simulations for micelles composed of 15 sodium octanoate molecules in water [39].

it is *assumed*—as already alluded to above—that the *prepared micelle* is stable. That is, in reality, a prepared aggregate can only lose its integrity on much longer time scales (e.g., micro- to milli-seconds). So the molecular dynamics computation falls short of being able to demonstrate the spontaneous formation and persistence of micelles with specific size and shape. Furthermore, many of the *structural* results mentioned below are quite sensitive to the uncertainties in molecular interaction parameters used in the calculations.

In spite of these numerous limitations, it is of interest to consider some of the reported MD results. In particular, the mean radius, derived from the positions of the head-group carboxylate oxygens, is found to be somewhat (15%) larger than the fully stretched (all-trans) chain length with a shape non-sphericity characterized by average principal inertial moment ratios of 1.7:1.5:1. Figure 1.5 shows the total carbon atom density profile, measured from the center of mass, as well as the density profiles for solvent water, head-group carbons, and sodium counterions. Note that the sodiums do not penetrate the core with water, but rather remain in the outer region with the carboxylate head groups. More significantly, *the simulation profiles serve to confirm the existence of a dry hydrophobic core.* (The "hole" at the micellar center is an artifact of the choice of system (box) size which leads to a small negative pressure.) The interfacial region in which water and alkyl segments are mixed is approximately 4Å wide,

compared to a micellar radius of roughly 12Å. Furthermore, the calculated bond conformational statistics and chain segment distributions are found to agree closely with the mean-field theory results to be discussed in Sec 1.3.3 and with the earlier model simulations by Pratt *et al.* [36] and Haile and O'Connell [37]. Recently, Karaborni and O'Connell [41a] have used molecular dynamics computations to examine the effects of alkyl chain length and head-group characteristics on internal micellar structure and chain packing. They confirm the existence of a well-defined, dry, hydrocarbon interior and of a significant degree of conformational disorder. Similar conclusions were reached by Wendoloski *et al.* [41b]; but again, we stress that these simulations—like those in [37–39]—begin with an already-assembled aggregate and, furthermore, treat the aqueous solvent only implicitly, via a set of effective "boundary forces."

Our interest in the above ideas concerning micellar structure lies primarily in their extension to larger aggregates having distinctly anisotropic shapes. As a rule it is found that average aggregation numbers begin to increase significantly at high enough concentrations (e.g., one to two orders of magnitude) above the CMC. The fact that at still higher concentrations one observes first *nematic* (rod- and disk-) liquid crystalline states and then hexagonal and lamellar *positionally ordered* phases, suggests further that the large aggregates in isotropic solution are themselves rod-like or disk-like. This conclusion is also consistent with the results described above, in our brief introduction to light scattering studies of isotropic phases, as well as in other chapters in this volume. Indeed, the very existence of large rod-like micelles in relatively dilute (i.e., ideal, as far as *inter*-aggregate forces are concerned) solution implies a strong self-assembly preference for cylindrical geometry. After all, if the hydrophobic effect could be satisfied equally well by spherical, rod-like, and disk-like aggregates, then the *minimum* (i.e., globular, spherical) micelle would be favored overwhelmingly. This is because the entropy of dispersion demands that—all other things being equal—the surfactants should organize themselves into the largest number of aggregates. But "all other things" are generally *not* equal, i.e., the *intra*-micellar ("self") free energy is distinctly lower for one particular geometry. Accordingly, one sees cylindrical aggregates predominating in dilute solutions of sodium decyl sulphate and other familiar surfactants, or essentially planar (bilayer) vesicles appearing in the case of phospholipid amphiphiles, and so on (see Chaps. 2 and 3). The fact that amphiphiles self-assemble into structures characterized by well-defined geometries provides additional support for the "standard" picture of the aggregates, as representing a well-defined hydrophobic region surrounded by a head-group mantle. Clearly, overall shape and surface roughness fluctuations do take place, but the basic structures are preserved.

As argued in the following sections, large aggregation numbers—commonly observed at high concentrations of surfactant and/or salt—can only be reconciled with *extended* structures. By extended aggregates we

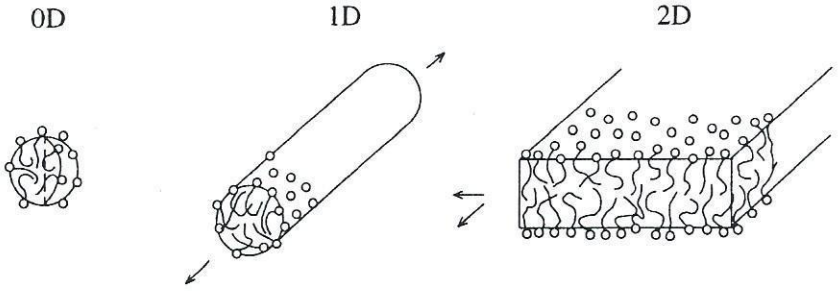

FIGURE 1.6. Schematic illustration of three "basic" aggregation geometries, describing aggregates that can grow along two dimensions (the bilayer), one dimension (the cylinder) and zero dimensions (i.e., no growth possibility, as for the spherical micelles).

mean those derived from minimum micelles via growth in one (rod) or two (disk) dimensions: see Fig. 1.6. Unlike the case of nucleation clusters [42–45] or microemulsion droplets (see Chaps. 7–9), the radius of a globular micelle can never significantly exceed the length of a fully stretched molecule; hence its "molecular weight" is restricted to small values. Accordingly, in the following sections we adopt as a basic premise the fact that big aggregation numbers are associated with a preference for cylindrical or bilayer packing of amphiphilic molecules. We explore the consequences of this premise on the equilibrium size distribution of aggregates and its dependence on concentration, and its consequences for phase transitions to orientationally and positionally long-range ordered states. This "first order" approach is all the more reasonable in light of the extreme difficulty of carrying out more detailed calculations on systems which necessarily involve so many degrees of freedom and such poorly understood interactions. The very few attempts to predict the spontaneous aggregation structures from basic statistical-thermodynamic principles have been necessarily limited to drastically simplified models (see, e.g., [46,47]). Thus we continue to characterize micelles by regular geometric structures, insofar as:

- a wide range of exotic self-assembly phenomena can be systematically explained within this description; and
- there still does not exist any compelling experimental or theoretical evidence which demands an alternative point of view.

1.2 Amphiphile Self-Assembly in Dilute Solutions

An equilibrium solution of amphiphiles in water corresponds (above the CMC) to a system of aggregates (micelles), generally of different sizes and possibly also different shapes, coexisting with a nearly constant concentration of monomers. Unlike in ordinary solutions, the solute particles (i.e., the micelles) in amphiphile solutions can respond to variations in thermodynamic parameters (such as total concentration, temperature or ionic strength) by changing their size and shape distributions. This behavior resembles that of a system governed by multiple chemical equilibria. The preferred aggregation geometry (e.g., spherical micelles, cylindrical aggregates or planar bilayers) and the equilibrium size distribution are determined by the molecular characteristics of the amphiphiles, as well as by the total concentration and other thermodynamic variables. In concentrated solutions, the sizes and shapes of the aggregates are also influenced by inter-aggregate forces, resulting in a rich and complex phase behavior, as discussed in Sec. 1.4 and in more detail in other chapters in this volume.

The discussion in this section is concerned with self-assembly and growth in the dilute solution regime. In Sec. 1.2.1 we introduce the basic statistical-thermodynamic concepts required to describe these phenomena, and in Sec. 1.2.2 we derive the formal expressions for the equilibrium size distribution. We then proceed to discuss the passage from monomers to aggregates (Sec.1.2.3), and to analyze the factors governing micellar growth with special emphasis on the role of the aggregate's dimensionality (Sec. 1.2.4). In Sec. 1.2.5 we briefly consider mixed aggregates and, finally, in Sec. 1.2.6 we comment on the contribution of external rotational and translational degrees of freedom to the micellar chemical potential, an issue which is totally overlooked in the phenomenological treatments of surfactant aggregation, and which still awaits a satisfactory statistical-thermodynamic resolution.

Before turning to the technical discussion, a few remarks should be made regarding the approach adopted here and its relation to alternative treatments. Throughout this chapter, rigorous statistical-thermodynamic derivations and concepts are interwoven with phenomenological descriptions. For instance, we employ elementary statistical thermodynamics to express the standard chemical potentials (which determine the equilibrium size distribution) in terms of the micellar partition functions. But then, realizing how difficult it is to treat rigorously the interactions determining the partition functions, we turn to phenomenological ('semi-empirical') considerations which, albeit approximate, provide important qualitative insights into the mechanisms of amphiphile association.

Many authors [48–55] have presented statistical-thermodynamic theories of micellar solutions, involving different degrees of rigor concerning, for example, the treatment of the solvent, the role of intra- and inter-micelle

interactions, or the effects of translational and rotational motions. Unfortunately, in many cases the ultimate results of such theories are formal expressions, e.g., for the partition functions, which are not very useful unless drastic approximations are invoked to simplify them. Other authors have formulated the micellization phenomena in terms of classical thermodynamics, treating micelles as small thermodynamic systems [56–59] ('micro-phases') and (some) analyzing in detail their mechanical properties [60,61]. The prevailing treatments of amphiphile self-assembly and micellar growth are those which combine basic classical thermodynamics with simple phenomenological models for the various contributions to amphiphile-amphiphile and amphiphile-water interactions [30–33,62–67]. One of our aims in the following discussion is to cast these notions into statistical thermodynamic terms, thus explicitly demonstrating the assumptions and approximations involved in the phenomenological approaches and thereby assessing their validity.

1.2.1 Underlying Statistical Thermodynamics

Consider a solution of N amphiphiles and N_w water molecules in volume V and at temperature T. At any given instant N_s of the N amphiphiles are incorporated in $n_s = N_s/s$ aggregates of size $s = 1, 2, \ldots$, with $\sum N_s = N$. $N_1 = n_1$ is, of course, the number of free monomers. Because of monomer association, micellar dissociation and exchange between aggregates, and similar dynamical processes involving groups of monomers or even micelles, the size distribution $\{n_s\}$ is a dynamical quantity, undergoing statistical fluctuations. Thus, the partition function of the system is a sum over all possible distributions of the amphiphiles: $Q_{tot}(N, N_w, V, T) = \sum_{\{n_s\}} Q_{tot}(\{n_s\}, N_w, V, T)$. (The subscript "*tot*" indicates 'total,' i.e., amphiphiles plus water.) However, the fluctuations around the average distribution $\{\bar{n}_s\}$ or, equivalently, the most probable distribution $\{n_s^*\}$, are negligible. Hence, using the usual maximum term method, we can safely replace $\ln Q_{tot}(N, N_w, V, T)$ by $\ln Q_{tot}(\{n_s^*\}, N_w, V, T)$ and express the Helmholtz free energy of the system as

$$A_{tot} = -kT \ln Q_{tot}(\{n_s^*\}, N_w, V, T) \tag{1.7}$$

The equilibrium size distribution corresponds to the set $\{n_s\} = \{n_s^*\}$ for which $\ln Q_{tot}(\{n_s\}, N_w, V, T)$ is maximal, so that A_{tot} is minimal. To derive $\{n_s^*\}$ we need an explicit expression for Q_{tot}. As a first step we separate A_{tot} into solvent and solute contributions. Assuming that the thermodynamic properties of the water are not affected by the presence of the micelles, one can write $Q_{tot}(\{n_s\}, N_w, V, T) = Q(\{n_s\}, V, T)Q_w$ and, correspondingly, $A_{tot} = A + A_w$. Here, $Q(\{n_s\}, V, T)$ is the partition function of the system of aggregates and monomers, dispersed in the continuous background of the solvent. The free energy of interaction between the micelles and the

aqueous solution is included in Q in a approximate fashion, as explained in Sec. 1.3. Q_w and A_w are the solvent contributions.

In dilute solutions, interaction effects between aggregates are negligible, and the free energy of a polydisperse system of $\{n_s\}$ aggregates is given, in analogy to ideal gas mixtures, by

$$\begin{aligned} A &= -kT \ln Q(\{n_s\}, V, T) = -kT \ln \prod_s \frac{q_s^{n_s}}{n_s!} \\ &= kT \sum_s n_s(-\ln q_s + \ln n_s - 1) \end{aligned} \tag{1.8}$$

where q_s is the partition function of an s-mer in solution. q_s includes contributions from the internal degrees of freedom of the aggregate, its overall translational and rotational motions, and approximately (via a potential of mean force) interaction effects with the solvent, as discussed in more detail in Secs. 1.2.6 and 1.3.1. It should be noted that the decomposition of Q and A into contributions from aggregates of different *sizes* does not imply that all s-aggregates are necessarily of identical *shape*. The possible existence of different micellar shapes, just like the possibility of small shape fluctuations, are included in q_s (in analogy to the case of a molecule fluctuating between several isomeric forms). Yet if one chooses to classify the aggregates by both size and shape, then Eq. (1.8) still holds, with s specifying both characteristics.

The derivation of $\{n_s^*\}$ from (1.8) is straightforward. However, we defer the derivation to the next section, after introducing several quantities, relationships and definitions which will prove useful later on. To this end we will temporarily regard (1.8) as the free energy of an ideal mixture of a given *fixed* composition $\{n_s\}$.

The chemical potential of species s is given by

$$\begin{aligned} \mu_s &= \left(\frac{\partial A_{tot}}{\partial n_s}\right)_{T,V,n_{s'\neq s},N_w} = \left(\frac{\partial A}{\partial n_s}\right)_{T,V,n_{s'\neq s}} \\ &= -kT \ln q_s + kT \ln n_s \\ &= -kT \ln(q_s/V) + kT \ln \rho_s \end{aligned} \tag{1.9}$$

with $\rho_s = n_s/V$ denoting the number density of s-aggregates. Combining (1.8) and (1.9), we find

$$\begin{aligned} A &= \sum_s n_s \mu_s - kT \sum_s n_s \\ &= G - \Pi V \end{aligned} \tag{1.10}$$

Here $G = \sum n_s \mu_s$ is the Gibbs free energy of the system of aggregates, not including the solvent's contribution. (The total Gibbs free energy of the solution is given by $G_{tot} = A_{tot} + PV = \sum n_s \mu_s + N_w \mu_w$. P is the

external pressure; $P = -(\partial A_{tot}/\partial V)$ with the derivative evaluated at constant composition.) Π is the osmotic pressure which, in the dilute solution limit, reduces to the ideal gas form $\Pi = kT(\sum \rho_s)$. It is easily verified that $\mu_s = (\partial G_{tot}/\partial n_s)_{T,P,N_{s'\neq s},N_w} = (\partial G/\partial n_s)_{T,\Pi,n_{s'\neq s}}$.

The chemical potential is conveniently expressed as

$$\mu_s = \mu_s^{o,\rho} + kT \ln \rho_s \tag{1.11}$$

with, cf. (1.9),

$$\mu_s^{o,\rho} = -kT \ln(q_s/V) = -kT \ln q_s^o \tag{1.12}$$

denoting the standard chemical potential "on the number density scale." Since the only volume dependent factor in q_s is the translational partition function, which is proportional to V, $q_s^o = q_s/V$ and consequently $\mu_s^{o,\rho}$ are functions of T only (see Secs. 1.2.6 and 1.3.1). While the number densities ρ_s are most convenient for statistical thermodynamic formulations, the predominant concentration scale in the phenomenological theories, as well as in the experimental literature on amphiphile self-assembly [30–33], involves the mole fractions, X_s, defined via

$$X_s = \frac{N_s}{N_{tot}} = \frac{sn_s}{N_{tot}}, \tag{1.13}$$

with $N_{tot} = N_w + N = N_w + \sum_s N_s$ denoting the total number of molecules, i.e., amphiphiles and water, in solution. Note that X_s is the mole fraction of amphiphiles incorporated into s-aggregates, as distinguished, say, from the mole fraction of s-aggregates $y_s = n_s/\sum n_s = (N_s/s)/\sum(N_s/s)$; $\sum y_s = 1$. Note also that the X_s do *not* sum up to 1, but instead

$$\sum_s X_s = X\ , \tag{1.14}$$

with $X = N/N_{tot}$ denoting the total mole fraction of amphiphiles in solution. In the dilute solution limit which is of interest here, $X = 1 - X_w \ll 1$, and $X_w \simeq 1$. X_s and ρ_s are related by

$$X_s = \frac{sn_s/V}{N_{tot}/V} = \frac{s\rho_s}{\rho_{tot}} \simeq \frac{s\rho_s}{\rho_w} \tag{1.15}$$

with $\rho_w = N_w/V$ and $\rho_{tot} = \rho_w + \sum s\rho_s$.

From (1.11), (1.12) and (1.15) we find

$$\mu_s = \mu_s^o + kT \ln(X_s/s) \tag{1.16}$$

where μ_s^o (which we use as a shorthand notation for $\mu_s^{o,x}$) is the standard chemical potential "on the mole fraction scale",

$$\mu_s^o = \mu_s^{o,\rho} + kT \ln\, \rho_{tot} = -kT \ln(q_s^o/\rho_{tot}). \tag{1.17}$$

In the dilute solution regime $\rho_{tot} \simeq \rho_w$ and $\mu_s^o (= \mu_s^{o,x})$ is independent of the amphiphile concentration X. In principle, however, since ρ_{tot} depends on X, so does μ_s^o (unlike $\mu_s^{o,\rho}$). Notwithstanding this reservation, in the following discussion we shall generally adopt the mole fraction scale, primarily in order to comply with the more familiar, phenomenological, treatments.

Using (1.13) and (1.16), the Gibbs free energy of the system (not including the solvent) can be expressed as

$$\begin{aligned} G &= \sum_s n_s \mu_s = \sum_s N_s \tilde{\mu}_s \\ &= N_{tot} \left[\sum_s X_s \tilde{\mu}_s^o + kT \sum_s (X_s/s) \ln(X_s/s) \right] \\ &\equiv G^o(\{X_s\}) - T\, S_d(\{X_s\}). \end{aligned} \tag{1.18}$$

The quantity

$$\tilde{\mu}_s \equiv \mu_s / s \tag{1.19}$$

will be referred to as the average chemical potential per amphiphile in an s-aggregate. Note in particular that $\tilde{\mu}_1 = \mu_1$ is the monomer's chemical potential. In analogy to (1.19) we define $\tilde{\mu}_s^o = \mu_s^o / s$.

The second term in (1.18), $S_d(\{X_s\})$, is an entropic contribution accounting for the 'dispersity' (or 'mixing') of the micellar size distribution. In particular, S_d is maximal when no aggregation takes place (i.e., when $X = X_1$ and $X_s = 0$ for all $s \geq 2$) demonstrating that micellization, like any aggregation process, is entropically unfavorable. More generally S_d is lowered by, and thus tends to oppose, any process which results in a smaller number (or lower polydispersity) of solute particles in the system. Thus, micellar *growth* is also an entropically unfavorable process. [It should be noted that $S_d(\{X_s\})$ involves only the so-called "mixing entropy" of the *solutes*. Solute-solvent mixing is not accounted for by S_d because G does not include the solvent contribution. Solute-solvent mixing is included in $G_{tot} = G + G_w = G + \sum N_w \mu_w$. The usual, ideal solution, mixing entropy results when we write $\mu_w = \mu_w^o + kT \ln X_w$, thus adding to (1.18) the solvent term $N_{tot} \sum X_w \mu_w^o + kT \sum X_w \ln X_w$ with $X_w = N_w / N_{tot}$.]

1.2.2 The Equilibrium Size Distribution

Expressed in terms of the mole fractions, X_s, the Helmholtz free energy A is given by (cf. (1.10), (1.13) and (1.16)),

$$A = N_{tot} \sum_s (X_s/s) \left[\mu_s^o + kT \ln(X_s/s) - kT \right] \tag{1.20}$$

As noted in the previous section the most probable distribution $\{X_s^*\}$ is the equilibrium size distribution, and $A(N, V, T, \{X_s^*\})$ is the free energy of the self-assembling amphiphilic system. The most probable distribution

corresponds to the set of X_s which minimizes A, subject to the conservation constraint $\sum X_s = X$. The conditional minimization can be carried out using the Lagrange multipliers method which, in our case, amounts to solving

$$\frac{\partial}{\partial X_s}\left(\frac{A}{N_{tot}} - \mu X\right) = 0 \ \ (\text{all } s) \tag{1.21}$$

with A given by (1.20). Here μ is the Lagrange multiplier conjugate to the constraint $X = \sum X_s$, with this later condition determining the numerical value of μ. The use of A/N_{tot} rather than A in (1.21) ensures that μ is intensive. This follows from the fact that A and $\mu X N_{tot} = \mu N$ must have the same dimensions and the same N-dependence, and that $A \sim N$. We shall soon see that μ is simply the amphiphile's chemical potential.

From (1.21), (1.20) and (1.14) we find that for all s

$$X_s^* = s \cdot \exp\left[-s\left(\tilde{\mu}_s^o - \mu\right)/kT\right] \tag{1.22}$$

The numerical value of μ can be determined by substituting (1.22) into $\sum\{X_s^*\} = X$ and solving the resulting equation for μ. Clearly, since the $\tilde{\mu}_s^o$'s depend on T only, it follows that $\mu = \mu(X,T)$. From (1.16), (1.19) and (1.22) we obtain

$$\begin{aligned} \mu &= \tilde{\mu}_s = \tilde{\mu}_s^o + (kT/s)\ln(X_s/s) \ \ (\text{all } s) \\ &= \mu_1 \end{aligned} \tag{1.23}$$

where it should be understood that here, and hereafter, all X_s stand for their most probable values X_s^*.

The last result reveals that μ is nothing else but the chemical potential of the amphiphiles in the solution which, at equilibrium, must be the same everywhere in the system. This includes free monomers, for which $\mu = \tilde{\mu}_1$, as well as amphiphiles incorporated in a micelle of (any) size s, for which $\mu = \tilde{\mu}_s$. Note also that, consistent with the general thermodynamic relation $G = N\mu$, the equality $\mu_s = s\tilde{\mu}_s = s\mu$ indicates that μ_s may be regarded as the Gibbs free energy of an s-aggregate. Of course, these are just different but equivalent interpretations of the equality

$$G = \sum_s n_s \mu_s = \mu \sum_s s n_s = N\mu \tag{1.24}$$

Another obvious and common interpretation of (1.23) derives from the notion that these equalities are the conditions for chemical equilibria in a system in which all the chemical reactions

$$sA_1 = A_s \ (\text{all } s)\,, \tag{1.25}$$

as well as linear combinations of these reactions (see below), take place simultaneously. In the present context A_s stands for an s-aggregate and

A_1 for a monomer. Of course one could start as well from (1.25) which implies $\mu_s = s\mu_1$ as the description of dynamical chemical (association-dissociation) equilibrium in the self-assembling solution. Then using (1.16) for μ_s we obtain the law of mass action [30–33,62–64]

$$\frac{(X_s/s)}{X_1^s} = \exp\left[s\left(\mu_1^o - \tilde{\mu}_s^o\right)/kT\right] \equiv K_s \tag{1.26}$$

Here X_s/s corresponds to the concentration of "product", and X_1 to that of "reactant" (raised to the power s, the "stoichiometric coefficient" in (1.25)); finally, $\mu_s^o - s\mu_1^o$ is the *standard free energy change* for the association "reaction." This "equilibrium quotient" result is entirely equivalent to (1.22), since $\mu = \mu_1 = \mu_1^o + kT \ln X_1$. Note, however, that this equivalence does not imply that the set of reactions (1.25) is the actual self-assembly mechanism in the system. (In fact the simultaneous association of s molecules to form an aggregate is a highly unlikely kinetic event.) The multiple chemical equilibria could similarly be described by other sets of independent (but coupled) reactions, e.g., the step-wise association processes

$$A_{s-1} + A_1 = A_s \tag{1.27}$$

for which $\mu_s = \mu_{s-1} + \mu_1$, consistent with (1.23). The equilibrium constants L_s corresponding to (1.27) are simply related to the K_s's, via

$$L_s = \frac{X_s/s}{X_1 X_{s-1}/(s-1)} = \frac{K_s}{K_{s-1}} \tag{1.28}$$

Clearly, this relation, as well as any other expression of the law of mass action corresponding to a set of independent chemical reactions such as (1.25) or (1.27), implies the same equilibrium values of X_s as those given by (1.22).

1.2.3 From Monomers to Aggregates—the CMC

The sudden appearance of micelles at a certain monomer concentration (the CMC) and the (near) constancy of the free monomer concentration upon further increase in the total amphiphile concentration (see Fig. 1.1), resemble a phase transition—in which the micelles play the role of a condensed phase and the free monomers the vapor (or the solute). This cooperative behavior indicates that even the smallest micelles formed contain a fairly large number of molecules, typically several dozens. The existence of some minimal aggregation number, m, can be explained by microscopic molecular packing considerations, as discussed in Sec. 1.3. In this section we shall only consider the thermodynamic implications of this fact.

As noted with regard to (1.18), the association of monomers into aggregates involves entropy loss. Thus, spontaneous aggregation must be associated with an "enthalpic" gain. More explicitly, from (1.22) or (1.26) we see

that unless $\tilde{\mu}_s^o < \mu_1^o$ (i.e., $K_s > 1$) for at least some $s > 1$, X_s will be much smaller than X_1 for all X and T. If only micelles of sizes $s \geq m$ appear, then clearly $\tilde{\mu}_s^o > \mu_1^o$ for all aggregates in the "gap" $2 \leq s \leq m$, whereas $\tilde{\mu}_s^o < \mu_1^o$ for $s \geq m$. The s-dependence of $\tilde{\mu}_s^o$ for $s \geq m$ determines the size distribution of the micelles as will be discussed in more detail in the next section. For our present goal, which is to characterize the CMC regime, it is both convenient and sufficient to assume for the moment that micelles of only one size, m, are formed in the system. Thus, the solution contains either free monomers at concentration X_1, or m-mers at concentration X_m, with $X_1 + X_m = X$. In terms of the $\tilde{\mu}_s^o$'s this scheme amounts to setting $\tilde{\mu}_s^o = \infty$ for all s except $s = 1$ and m; it corresponds, approximately, to a system of amphiphiles whose overwhelmingly preferred aggregation geometry is spherical (Secs. 1.2.4 and 1.3.2).

The onset of micelle formation and the corresponding saturation of the free amphiphile concentration takes place over a narrow (yet finite) range of the total concentration X. Thus, any X or X_1 in this range may be taken as an operational definition of the CMC. Generally, we can specify the CMC as the (monomer or total) concentration corresponding to a solution in which a certain fraction σ of the amphiphiles are micellized. (It is common [30] to use $\sigma \approx 0.01 - 0.1$; yet, larger values, e.g., $\sigma = 1/2$ are also common and for mathematical purposes are often more convenient.) Let us denote by $\hat{X} =$ CMC, $\hat{X}_1 = (1-\sigma)\hat{X}$ and $\hat{X}_m = \sigma\hat{X}$, the critical values of the total, free and micellized amphiphile concentrations, respectively. Then from (1.26) we get

$$\begin{aligned} \ln(CMC) &= -\left(\frac{m}{m-1}\right)\left(\mu_1^o - \tilde{\mu}_m^o\right)/kT + \frac{1}{m-1}\ln\left[\frac{\sigma}{m(1-\sigma)^m}\right] \\ &\approx -\left(\mu_1^o - \tilde{\mu}_m^o\right)/kT \end{aligned} \tag{1.29}$$

In passing to the second equality we have taken into account that, typically, $m \simeq 20 - 100$ [30–33]. Neglecting the second term in the first equality is justified (for all reasonable σ) since generally $(\mu_1^o - \tilde{\mu}_m^o)/kT \geq 10$. Choosing σ to be small implies that the free monomer concentration and the CMC are the same, i.e.,

$$\hat{X}_1 \approx \text{CMC} \approx \exp\left[-\left(\mu_1^o - \tilde{\mu}_m^o\right)/kT\right] \tag{1.30}$$

To demonstrate the sharpness of the transition from free monomers to micelles at the CMC we first use (1.26) to write

$$X_m = X - X_1 = \hat{X}_m\left(X_1/\hat{X}_1\right)^m \tag{1.31}$$

Using $\hat{X}_1/\hat{X}_m = (1-\sigma)/\sigma$ we find

$$\frac{\partial X_1}{\partial X} = \left[1 + \alpha\left(\frac{X_1}{\hat{X}_1}\right)^{m-1}\right]^{-1} \tag{1.32}$$

where $\alpha = m\sigma/(1-\sigma)$ is of order 1. This very simple relation shows clearly how the fact that $m \gg 1$ is reflected in the monomer concentration. Below the CMC, i.e., as long as $(X_1/\hat{X}_1) < 1$, the second term in the denominator on the r.h.s. (right hand side) of (1.32) is negligible, so that $\partial X_1/\partial X \approx 1$ and $X_1 \approx X$, i.e., all the amphiphiles are free monomers. On the other hand, once X_1 exceeds, even slightly, its CMC value $\hat{X}_1$, we find $\partial X_1/\partial X \sim (\hat{X}_1/X_1)^{m-1} \approx 0$, and hence $X_1 \approx \hat{X}_1 =$ constant. As a numerical example consider, say, a surfactant (not very different from SDS) for which CMC $\approx \hat{X}_1 = 10^{-5}$ and $m = 50$ (suppose $\sigma \approx 0.1$ so that $\hat{X}_1 \approx 10\hat{X}_m$). It follows from (1.31) that when $X_1 = 0.9\hat{X}_1$ for instance, $X_m \approx 10^{-4}\hat{X}_1$ is still negligible. On the other hand, even at very high concentrations, e.g., $X = 1000$ CMC $= 1000\hat{X}_1$, the monomer concentration has only increased to $X_1 \approx 1.15\hat{X}_1$.

Most of the free energy gain associated with amphiphile packing in a micelle reflects the preference of the amphiphile's hydrocarbon chain for the hydrophobic environment inside the micellar core, as compared to the aqueous environment of the free amphiphile. The CMC or, equivalently, the saturation concentration (solubility limit) of free monomers, decreases exponentially with this preference which is measured by $\Delta\tilde{\mu}^o = \mu_1^o - \tilde{\mu}_m^o$: see (1.30). For most amphiphiles $\Delta\tilde{\mu}^o$ increases nearly linearly with the amphiphile chain length [30].

It should be noted that relative to $\hat{X}_1$, the sharpness of the monomer-micelle transition depends entirely on m. However, the absolute width, i.e., the concentration range characterizing the transition, depends on $\hat{X}_1$ as well. The lower is the CMC, the sharper is the transition. The dependence on m reflects the *cooperativity* of the transition. As m increases, the transition resembles more closely a real, first order phase transition, in which the micelles correspond to a condensed phase, and the monomers are the vapor. Several treatments of micelle formation are based on this analogy [57–59]. Such treatments can account for the behavior at the CMC and for monomer-aggregate coexistence. On the other hand, since the micelles are regarded as macroscopic phases, the size dependence of their thermodynamic properties is necessarily ignored (corresponding to $S_d \equiv 0$ in (1.18)). Consequently, this "microphase" view of the micelle is, for instance, inadequate for discussing micellar growth.

Although the above technical discussion has been limited for convenience of illustration to a monodisperse micellar system, all the qualitative conclusions remain valid when larger micelles are also possible. We shall comment briefly on this point in the next section.

1.2.4 Micellar Growth

Micellar aggregates appear in various shapes and sizes, depending on the molecular nature of the constituent amphiphiles (Sec. 1.3) as well as on the total concentration and other thermodynamic parameters. There is,

however, one basic structural feature commonly shared by all aggregates: the width (diameter) of their hydrophobic core is always on the order of the amphiphile's molecular length. More precisely, since holes within the hydrophobic region are energetically intolerable, the core diameter cannot exceed $2l$ where l is the length of the fully stretched hydrocarbon tail, cf. Fig. 1.6. Consequently, at least one linear dimension of the hydrophobic core in all aggregates is of order l. This simple notion is essential for understanding micellar growth, and suggests a classification of the aggregates into three general categories as follows:

1. Globular aggregates—in which all three linear dimensions are of order l. A spherical micelle of radius $R \leq l$ can serve as a prototype of this class.

2. Rod-like aggregates—in which two dimensions, those perpendicular to the long (rod) axis, are of order l. A cylindrical micelle of radius $R \leq l$ and length $h > 2l$ is the typical example of this class. Such micelles are often described as spherocylinders, i.e., as cylinders capped by hemispheres at their two ends (Fig. 1.6). As we shall see below, end effects play an essential role in micellar growth; however, the structural details of the ends are (qualitatively) irrelevant.

3. Bilayers—in which only one dimension is of order l, namely, the thickness, which cannot exceed $2l$. An oblate, disk-like aggregate of thickness $w \approx 2l$ and diameter $h > 2l$ can serve as a representative of this class. Again, a more specific geometry (e.g., a disk-shaped body surrounded by a semi-toroidal rim) may be assumed for these aggregates; however, as with rod-like micelles, their growth characteristics are governed by their dimensionality and not by structural details.

Quite generally, micellar growth is driven by the tendency to reduce unfavorable end ("edge" or "surface") effects. In particular, we shall see that above a certain concentration disk-like micelles tend to grow, actually to undergo a phase transition, to infinitely large sheet-like aggregates. Another possibility for bilayers to overcome the excess rim energy is to close upon themselves and hence to form spherical vesicles [30–33]. (Similarly, rod-like micelles can close into tori [66].) Vesicles serve as model systems for biological membranes and are interesting entities in their own right. However, unlike spherical, cylindrical and disk-like aggregates whose growth characteristics are dictated by the dimensionality and end effects which we want to emphasize here, other factors control the size behavior of vesicles, primarily curvature elasticity (Sec. 1.3.3). Thus, except briefly in Sec. 1.2.5, we shall not discuss vesicles in this chapter.

1.2.4.1 The phenomenological approach [30–33]

As noted already in Secs. 1.2.1 and 1.2.3, micellar growth, like any other aggregation process in dilute solution, reduces the translational ("mixing")

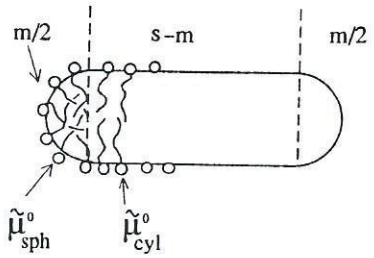

FIGURE 1.7. Schematic illustration of a rod-like micelle, described as a simple sphero-cylinder.

entropy of the system. For growth to occur, the *internal* free energy per molecule within the aggregate must decrease with size; that is, $\tilde{\mu}^o_s$ must decrease as s increases. Consider for example a spherocylindrical rod-like micelle of s amphiphiles, of which $m/2$ comprise each of the two hemispherical ends and $s-m$ constitute the cylindrical body, cf. Fig. 1.7. Clearly, such micelles tend to grow if the molecules feel more "comfortable" in a cylindrical rather than in a spherical environment. This is more quantitatively expressed by the inequality $\tilde{\mu}^o_{cyl} < \tilde{\mu}^o_{sph}$, with $\tilde{\mu}^o_{cyl}$ and $\tilde{\mu}^o_{sph}$ denoting the average free energy (standard chemical potential) of the molecules packed in cylindrical and spherical environments, respectively. We similarly define $\tilde{\mu}^o_{bil}$ as the free energy per amphiphile in a planar bilayer.

The $\tilde{\mu}^o_g$ ($g = sph, cyl, bil$) play a central role in the phenomenological approach to micellar growth which we follow largely in this section [30–33,62–66]. In particular, this approach provides a simple way to analyze the dependence of micellar sizes on the competition between the tendency of molecules to organize into larger aggregates (when $\tilde{\mu}^o_{sph} > \tilde{\mu}^o_{cyl}$ or $\tilde{\mu}^o_{cyl} > \tilde{\mu}^o_{bil}$) and the accompanying loss in translational entropy. Note that larger aggregates also correspond to lower (average) curvature of the hydrocarbon-water interface. The $\tilde{\mu}^o_g$ depend on the molecular characteristics of the amphiphiles, and can be calculated from molecular models or inferred from experimental data (see Sec. 1.3). In the present discussion we shall be mainly concerned with their relative magnitudes.

A key assumption in the phenomenological approach is that μ^o_s of an arbitrary aggregate can be expressed as a superposition of the $\tilde{\mu}^o_g$'s corresponding to its different microenvironments. That is,

$$\mu^o_s = \sum_g s_g \tilde{\mu}^o_g \tag{1.33}$$

with s_g denoting the number of molecules in microenvironment g. For example, for the spherocylindrical micelle containing $s - m$ molecules in the

cylindrical body and $m/2$ molecules in each hemispherical end (Fig. 1.7), we have

$$\begin{aligned} \mu_s^o &= s\tilde{\mu}_s^o = (s-m)\tilde{\mu}_{cyl}^o + m\tilde{\mu}_{sph}^o \\ &= s\tilde{\mu}_{cyl}^o + m\left(\tilde{\mu}_{sph}^o - \tilde{\mu}_{cyl}^o\right) \quad (s \geq m) \end{aligned} \tag{1.34}$$

Similarly, for a disk-like micelle, μ_s^o can be expressed as a linear combination of $\tilde{\mu}_{bil}^o$ and $\tilde{\mu}_{rim}^o$ corresponding, respectively, to the $s-k$ molecules in the central part, and the k molecules in the semi-toroidal rim (which for large s becomes semi-cylindrical [68], i.e., $\tilde{\mu}_{rim}^o = \tilde{\mu}_{cyl}^o$, and $k \sim s^{1/2}$). More generally, for a (large) d-dimensional aggregate, we can write

$$\mu_s^o = s\tilde{\mu}_s^o = s\tilde{\mu}_\infty^o + kT\,\delta s^{(d-1)/d} \tag{1.35}$$

Here $\tilde{\mu}_\infty^o = \mu_{s\to\infty}^o$ denotes the asymptotic standard chemical potential, i.e., the free energy per molecule in the main body of the aggregate and δkT is a measure of the excess edge ("surface") free energy. Note that both $\tilde{\mu}_\infty^o$ and δ depend on the aggregate's dimensionality (or, more precisely, on its geometry), e.g., for spherocylinders $(d=1), \tilde{\mu}_\infty^o = \tilde{\mu}_{cyl}^o$ and $\delta = m(\tilde{\mu}_{sph}^o - \tilde{\mu}_{cyl}^o)/kT$. A relation similar to (1.35), known as the "capillarity approximation", is used in nucleation theory for the standard chemical potential of a nucleation cluster [42–45]. In nucleation problems, one is mainly concerned with $d=3$, in which case $\tilde{\mu}_\infty^o$ is identified as the "bulk" chemical potential corresponding to the interior of the cluster, while the second term in (1.35) accounts for the surface free energy, i.e., $\delta s^{2/3} \sim 4\pi R^2\gamma$, where R is the cluster's radius and γ is the surface tension. (Note that, in general, for a d-dimensional cluster of radius R, the "volume" varies as $R^d \sim s$ and the "surface" as $R^{d-1} \sim s^{(d-1)/d}$.)

1.2.4.2 Dimensionality and micellar growth

Since at least one linear dimension of a micelle is restricted to be of order l, micellar growth is limited to either $d=1$ (as in rod-like micelles) or $d=2$ (planar, or disk-like aggregates). Based on the expressions derived for X_s in Sec. 1.2.2 and the simple relation (1.35), one can show that micellar growth in $d=1$ and $d=2$ (or, more generally, $d>1$) are markedly and qualitatively different from each other. In particular, we shall see that for $d=2$ a first-order phase transition from finite micelles (or even directly from monomers) to infinite aggregates takes place at some low amphiphile concentration, $\bar{X}$. On the other hand, for $d=1$, the average micellar size varies continuously with X and remains finite at all concentrations.

Let us first derive the condition for coexistence between a saturated (albeit dilute) solution containing monomers and finite micelles, and an infinite aggregate which, thermodynamically, constitutes a macroscopic condensed phase. According to the capillarity approximation and the phenomenological approach described above, the amphiphile chemical potential (i.e., the free energy per molecule) in the infinite aggregate is $\tilde{\mu} = \tilde{\mu}_\infty^o$.

If these aggregates coexist in equilibrium with the monomers and finite micelles, then $\tilde{\mu}^o_\infty = \mu_1 = \tilde{\mu}_s$ and hence

$$\begin{aligned} \tilde{\mu}^o_\infty &= \mu^o_1 + kT \ln \bar{X}_1 \\ &= \tilde{\mu}^o_s + (kT/s) \ln(\bar{X}_s/s) \quad (s \geq m) \end{aligned} \tag{1.36}$$

with $\bar{X}_1$ and $\bar{X}_s/s$ denoting the concentrations of monomers and s-micelles at saturation. For further reference we rewrite the first equality in (1.36) as

$$\bar{X}_1 = \exp\left[-\left(\tilde{\mu}^o_1 - \mu^o_\infty\right)/kT\right] . \tag{1.37}$$

For the second equality we use (1.35) to obtain

$$\bar{X}_s = s \cdot \exp\left[-\delta s^{(d-1)/d}\right] \quad (s \geq m) \tag{1.38}$$

Now the difference between $d = 1$ and $d = 2$ (or any $d > 1$) is apparent. The sum

$$\bar{X} = \bar{X}_1 + \sum_{s=m}^{\infty} \bar{X}_s \tag{1.39}$$

converges to a finite total concentration $\bar{X}$ for $d = 2$, but *diverges* for $d = 1$. Since (1.36) cannot be satisfied for $d = 1$, the conclusion is that an infinitely long, one-dimensional, aggregate cannot coexist with an ideal solution of finite, rod-like, micelles. Conversely, as we shall see below, for $d = 1$ the condition $X = X_1 + \sum X_s$ can be satisfied for all X, with the appropriate X_s for finite rod-like micelles in dilute solutions. (Recall, however, that the discussion here is limited to the dilute solution regime, where interaction effects between micelles are negligible; see Sec. 1.4.)

Consider now the $d = 2$ case (the conclusions apply to all $d > 1$). Below saturation, i.e., when $X < \bar{X}$, the solution contains only monomers or finite micelles, because $\tilde{\mu}_s < \tilde{\mu}^o_\infty$ for $X_s < \bar{X}_s$; see (1.36). When $X > \bar{X}$ a saturated dilute solution of monomers and micelles (with $X_s = \bar{X}_s$) coexists with infinite two dimensional bilayer lamellae containing all the other $(X - \bar{X})$ amphiphiles: adding more amphiphiles just leads to more bilayers, without affecting the micellar size distribution $\{\bar{X}_s\}$. Thus, $\bar{X}$ marks the onset of a first-order phase transition. Note, finally, that for disk-like micelles the surface term in (1.35), hence in (1.38), varies as $s^{1/2}$ because we have assumed large s (e.g., $s > 100$); for smaller sizes the dependence on s is more complicated [68]. In practice, these details are irrelevant because for systems of bilayer-forming amphiphiles (for which $\tilde{\mu}^o_{bil} < \tilde{\mu}^o_{sph}, \tilde{\mu}^o_{cyl}$) $\bar{X}$ is generally negligible compared to the total amphiphile concentrations of interest. (E.g., for long chain phospholipids $\delta > 5$ and $m > 50$, implying extremely small $\bar{X}_s$ for all $s > m$. Furthermore, for these molecules $\tilde{\mu}^o_1 - \mu^o_\infty > 20$, implying negligible $\bar{X}_1$; see (1.37)).

The different qualitative behaviors of $d = 1$ and $d > 1$ aggregates reflect inverse "hierarchies" of the "surface free energy" and the translational entropy contributions to $\tilde{\mu}_s$. Although this important point may already be

clear from the discussion above, let us consider it from a more explicit approach, in the spirit of the analysis of Landau and Lifshitz [69]. To simplify the discussion, we again suppress the effects of polydispersity, assuming that all micelles are of one size s, hence $X_{s'} = \delta_{ss'} X$. (We also ignore the monomers, which are irrelevant for micellar growth; see below.) Thus, using (1.23) and (1.35), we have

$$\begin{aligned} \tilde{\mu}_s &= \tilde{\mu}_s^o + (kT/s)\ln(X/s) \\ &= \tilde{\mu}_\infty^o + kT\,\delta s^{-1/d} + (kT/s)\ln(X/s)\,. \end{aligned} \tag{1.40}$$

Hence,

$$\frac{\partial \tilde{\mu}_s}{\partial s} = \frac{kT}{s^2}\left[-bs^{(d-1)/d} + \ln\left(\frac{s}{eX}\right)\right] \tag{1.41}$$

with $b = \delta/d$.

Consider first the $d > 1$ case. For large enough s, say $s > \bar{s}$, the first term in the square brackets, corresponding to the decrease in surface free energy of the system (per molecule) is larger than the second term, $\ln(s/eX)$, which accounts for the loss of translational entropy as s increases. Hence, beyond $\bar{s}$, $\tilde{\mu}_s$ falls off without bound ($\partial\tilde{\mu}_s/\partial s < 0$), reflecting the tendency of the amphiphiles to form infinite aggregates. (For $d = 2$ and typical values such as $b \approx 5$ and $X \approx 10^{-3}$ one finds that $\tilde{\mu}_s$ starts decreasing already above $\bar{s} \approx 3$.) On the other hand, for $d = 1$ the surface term is constant, hence $\partial\tilde{\mu}_s/\partial s = kT/s^2[-b+\ln(s/eX)]$ vanishes (corresponding to the state of minimum free energy) for a *finite* aggregation number, $s = X\exp(\delta+1)$. In other words, no matter how large the growth parameter (the "surface free energy"), or the total concentration X, the entropic contribution is always sufficient to keep the micelles finite. This is a striking manifestation of the "theorem" concerning "the impossibility of the existence of phases in a one dimensional system" [69].

We now turn to consider the polydispersity of micellar sizes. There is little to say about disk-like ($d = 2$) micelles, whose size distribution reaches its saturation value, as given by the $\bar{X}_s$ of (1.38), already at low concentrations. On the other hand, rod-like micelles are characterized by a broad and X-dependent size distribution, as discussed in the next section. The main results obtained there are well known [31–33,53,63–68], but the presentation and emphasis are somewhat different.

1.2.4.3 From short to long micelles—the "sphere-to-rod transition" [31, 64–66]

We consider a solution of amphiphiles preferentially aggregating into rod-like micelles, which for the sake of concreteness will be treated as spherocylinders; see Fig. 1.7. Thus, we express $\tilde{\mu}_s^o$ as in (1.34) or equivalently (1.35) with $d = 1$. Upon substitution into either of the general expressions (1.26) or (1.22), X_s can be rewritten in the simple form

$$X_s = se^{-(\alpha s+\delta)} \quad (s \geq m) \tag{1.42}$$

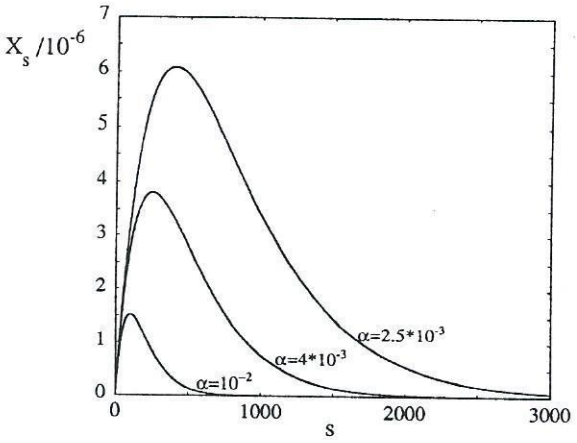

FIGURE 1.8. Size distribution of rod-like micelles in dilute solution, calculated using Eq. (1.42) for $\delta = 15, m = 50$, and three values of α. The total concentrations corresponding to $\alpha = 10^{-2}, 4 \times 10^{-3}$ and 2.5×10^{-3} are $X = 3.77 \times 10^{-4}, 2.54 \times 10^{-3}$ and 6.57×10^{-3}, respectively.

with $\delta = m(\tilde{\mu}^o_m - \tilde{\mu}^o_\infty)/kT > 0$ denoting the rods' growth parameter. (Note that $\tilde{\mu}^o_m = \tilde{\mu}^o_{sph}$ and $\tilde{\mu}^o_\infty = \tilde{\mu}^o_{cyl}$.) The quantity α can be expressed in several different but equivalent forms; e.g.,

$$\begin{aligned} \alpha &= 1/s^* = (\tilde{\mu}^o_\infty - \mu)/kT \\ &= \ln(\bar{X}_1/X_1) = (1/s)\ \ln(\bar{X}_s/X_s) \end{aligned} \tag{1.43}$$

The first equality identifies $1/\alpha$ as s^*, the most probable aggregation number, as follows directly from $\partial X_s/\partial s = 0$ and (1.42). In the second equality μ is the chemical potential of amphiphiles in solution, cf. (1.22) and (1.23). In the third and fourth equalities, α is related to the limiting ("saturation") concentrations of monomers, $\bar{X}_1$, and s-micelles, $\bar{X}_s$, respectively, cf. (1.36). From the discussion in the previous section we know that a solution of rod-like micelles ($d = 1$) is never saturated. Thus, as X increases, all X_s approach $\bar{X}_s$ very closely but never quite reach these values. Correspondingly α is positive and approaches zero as X increases. A typical progression of X_s-distributions, upon increasing X, is shown in Fig. 1.8. Given the very simple form of X_s in (1.42), one can easily calculate any desired characteristic of the size distribution, such as the averages $\langle s \rangle$, $\langle s^2 \rangle$, etc. The monomer contribution to these quantities can be included explicitly and exactly. However, for a number of reasons we prefer to completely ignore the monomer terms in the discussion of micellar growth. First, this simplifies all derivations. Second, we are explicitly interested in concentrations

well above the CMC where the monomer concentration is both negligible and essentially constant, i.e., $X \gg X_1 \approx \bar{X}_1 = constant$. To see this more clearly, we note that in this concentration regime $\hat{X}_1 < X_1 < \bar{X}_1$, with $\hat{X}_1$ denoting the monomer concentration at the CMC as given by (1.30), and $\bar{X}_1$ the limiting concentration (1.37). (From (1.30) and (1.37) we find $\hat{X}_1/\bar{X}_1 \sim \exp(-\delta/m)$ with δ/m ranging typically between 0.1 and 0.5.) We shall see below that at high concentrations $s^* \approx \langle s \rangle \approx 1/\alpha \gg 1$, hence $X_1/\bar{X}_1 = \exp(-\alpha) \approx \exp(-1/s^*) \approx 1$. Finally, we note that although X_s is often expressed in terms of X_1 (see e.g., (1.26)), the monomers have no influence on the micellar size distribution. This is because the growth of spherical into cylindrical micelles, which is sometimes called "the sphere-to-rod transition", is governed completely by the two parameters δ and α; δ measuring the difference in free energy between spheres and cylinders and α reflecting the total concentration. None of these parameters depend on monomer properties!

The kth moment of X_s is defined by

$$\begin{aligned} M_k &= \sum_{s \geq m} s^k X_s = e^{-\delta} \sum_{s \geq m} s^{k+1} e^{-\alpha s} \\ &= e^{-\delta} \left(-\frac{\partial}{\partial \alpha} \right)^{k+1} \sum_{s \geq m} e^{-\alpha s} \\ &\approx e^{-\delta} (k+1)!/\alpha^{k+2} \end{aligned} \tag{1.44}$$

where in the second equality we have used (1.42). In the passage to the last equality we have used the approximation $\sum_{s \geq m} \exp(-\alpha s) = \exp(-\alpha m)/(1 - \exp(-\alpha)) \approx 1/\alpha$, corresponding to the assumption $\alpha m = m/s^* \ll 1$. Based on this last assumption, we shall replace below the summations $s \geq m$ by $s \geq 0$.

The zeroth moment is simply the *total* amphiphile concentration, $M_0 = \sum X_s = X - X_1 \approx X = \exp(-\delta)/\alpha^2$. From M_1 we obtain the familiar result for the *weight averaged* size [31,32,63,64,66,70]

$$\begin{aligned} \langle s \rangle_w &= \sum_s s X_s / \sum_s X_s = 2/\alpha = 2s^* \\ &= 2(X e^{\delta})^{1/2} \end{aligned} \tag{1.45}$$

Similarly, for the *width* of the micellar size distribution we obtain

$$\begin{aligned} \sigma_s &= \left[\langle s^2 \rangle_w - \langle s \rangle_w^2 \right]^{1/2} = \langle s \rangle_w / \sqrt{2} \\ &= (X e^{\delta}/2)^{1/2} \end{aligned} \tag{1.46}$$

indicating significant size polydispersity, as reflected in Fig. 1.8.

Weight averages are calculated with respect to the "weight distribution", $P_w(s) = X_s/X$, expressing the fraction of molecules incorporated in micelles of size s. Similarly, *number* averages are calculated using the "number

distribution", $P_n(s) = n_s / \sum n_s = (X_s/s)/\sum(X_s/s)$, corresponding to the fraction of micelles of size s. Thus, the number averaged size is defined and given by

$$\begin{aligned} \langle s \rangle_n &= \sum_s s(X_s/s)/\sum_s (X_s/s) = M_0/M_{-1} \\ &= 1/\alpha = \langle s \rangle_w /2 = s^* \end{aligned} \tag{1.47}$$

Combining (1.42) and (1.47), we find

$$P_n(s) = \frac{1}{\langle s \rangle_n} \exp\left[-s/\langle s \rangle_n\right] \tag{1.48}$$

with $\sum P_n(s) \approx \int P_n(s)ds = 1$.

The analogous expression for $P_w(s) = X_s/X$ reads

$$P_w(s) = \frac{4s}{\langle s \rangle_w^2} \exp\left[-2s/\langle s \rangle_w\right] \tag{1.49}$$

which is another form of (1.42), appropriate for $\langle s \rangle_w \gg m$.

The basic characteristics of 1D micellar growth in dilute solution have been confirmed by many experiments. For instance, light scattering measurements [7,10] of the average size (hydronamic radius, $\bar{R}_H$) of ionic (e.g., SDS) micelles corroborate (1.45). In particular, from plots of $\bar{R}_H$ vs. T it has been possible to deduce the growth parameter δ for different values of the total salt (NaCl) concentration in the solution. The Coulomb repulsion between surfactant head-groups is partially screened by the added counterions. Thus, the added salt favors more strongly the cylindrical over the spherical packing environment (see Sec. 1.3.2), implying larger $\delta = m(\tilde{\mu}^o_{sph} - \tilde{\mu}^o_{cyl})/kT$ and larger micellar sizes. The above experiments enable quantitative evaluation of δ, which for SDS is ≈ 20.

Deviations from the simple rod growth model described in this section are obviously expected at high surfactant concentrations, where aggregation numbers are large and inter-micelle forces are no longer negligible (see Sec. 1.4). However, deviations are also expected in dilute solutions whenever μ^o_s is not exactly a linear function of s. This, for example, may be the result of curvature effects on the electrostatic interactions in ionic surfactant solution [71], the addition of cosurfactants, or the flexibility of large "worm-like" micelles [78–81]. These issues as well as a more detailed account of experimental results are discussed by Porte in the next chapter (see also Sec. 1.2.5 below).

1.2.5 Other Aggregates

The discussion in Sec. 1.2.4 has been focused on the role of dimensionality in micellar growth. Accordingly, we have considered only three basic

aggregation geometries: spheres, cylinders and planar bilayers, and their "combinations"—e.g., as spherocylinders or disk-like micelles with semi-toroidal rims. Furthermore, it has been assumed that all aggregates in solution have the same geometry. Clearly, this is an approximation, and the possibility that aggregates of different shapes, e.g., rod-like and disk-like, can co-exist in solution must be taken into account.

To examine the above possibility, let us consider two aggregation geometries g and g'. (The symbol g has been previously used, e.g., in (1.33), to denote a "basic" geometry such as *sphere* or *cylinder*. Hereafter, we shall also use it for "complex" geometries such as *spherocylinders*.) From (1.22) or (1.26) one expects that if the free energy per molecule in the two geometries is similar (yet not strictly equal), namely $\tilde{\mu}^o_{s,g} \approx \tilde{\mu}^o_{s,g'}$, then $X_{s,g} \approx X_{s,g'}$, i.e., the solution will contain similar numbers of s,g and s,g'-aggregates. This conclusion is valid for small s only; *for large s there will always be a single dominant geometry.* This can be understood quite generally using (1.35) from which it follows that for large s, $\Delta\mu^o_s = \mu^o_{s,g'} - \mu^o_{s,g} \approx s[\tilde{\mu}^o_{\infty,g'} - \tilde{\mu}^o_{\infty,g}] \equiv s\Delta\tilde{\mu}^o_\infty$, where we have neglected the surface term in μ^o_s. (Recall that $\tilde{\mu}^o_{\infty,g}$ is the chemical potential in the main part of the aggregate, e.g., for $g = rod$, $\tilde{\mu}^o_{\infty,g} = \tilde{\mu}^o_{cyl}$ and for $g' = disk$, $\tilde{\mu}^o_{\infty,g'} = \tilde{\mu}^o_{bil}$.) Now, suppose for concreteness that $\Delta\tilde{\mu}^o_\infty = \tilde{\mu}_{\infty,g'} - \tilde{\mu}^o_{\infty,g} > 0$, i.e., g is the (asymptotically) more stable geometry. Clearly, even if $\Delta\tilde{\mu}^o_\infty$ is not large compared to kT, this ("monomeric") difference is largely magnified when comparing large aggregates, for which $\Delta\mu^o_s = s\Delta\tilde{\mu}^o_\infty \gg kT$, implying $X_{s,g'}/X_{s,g} = \exp[-\Delta\mu^o_s/kT] \ll 1$.

Free energy differences corresponding to amphiphile packing in different aggregation geometries, $\Delta\tilde{\mu}^o_\infty$, are typically a few tenths of kT [30–33]. Thus, if e.g., $\Delta\tilde{\mu}^o_\infty/kT \approx 0.1$ then already for $s \approx 100$ one expects a single geometry to prevail. However, for these low aggregation numbers one also has to consider the contribution of the surface terms (cf. (1.35)) which have been ignored in the above analysis. Theoretical analyses indicate that in some systems, at low concentrations, when the micelles are typically small, the solution contains different micellar shapes, e.g., oblate (or disk-like) and prolate (or rod-like) particles [68]. It is also possible that a cross-over from dominance by one geometry to another will take place at some range of concentration and hence of micellar sizes [55,68,82]. However, since these behaviors concern small aggregates they are very difficult for experimental measurements to probe.

The (possible) appearance of micellar aggregates in different geometries may also be regarded as shape fluctuations of these complex particles. Thus, not surprisingly, such fluctuations are expected to be more pronounced when the aggregates are small. Shape fluctuations of different kinds are also observed for large micelles. Of particular interest in this context are the "giant" rod-like micelles which, similar to polymers, show a high degree of flexibility, and are often described as "*worm-like*" micelles. For these aggregates the form (1.34), for the standard chemical potential of a (rigid)

rod-like aggregate, should be extended to include contributions accounting for the conformational flexibility of the micelle [66]: see Sec. 2.2.3.

Semi-flexible rod-like micelles (even relatively short or somewhat rigid ones) can bend so that their ends fuse, thus forming a ring (torus) shaped aggregate. The bending free energy associated with the formation of the ring (see Sec. 1.3.4) provides a positive, hence unfavorable, contribution to μ_s^o. Furthermore, ring closure involves a loss of conformational entropy. On the other hand, the ring closure relieves the unfavorable free energy price corresponding to the two ends, cf. (1.34). Since this last term is the driving force for the growth of rod-like aggregates, it is clear that the relative abundance of rings and rods will be determined by the difference between the bending and the edge free energies [66].

A more interesting case where "bending and fusion" relieves unfavorable edge free energy corresponds to the formation of *vesicles*, i.e., bilayers which close upon themselves to form a nearly spherical bubble [30–33,53,83–87]. Recall from Sec. 1.2.4 that large planar disk-like micelles are unstable. Thus vesicle formation not only relieves the excess free energy associated with the rim of a disk-like micelle, but also allows for the possibility of finite aggregates composed of (non-planar) bilayers. As usual, the size distribution of vesicles in dilute solution is determined by the variation of μ_s^o with s, which correlates with the vesicular radius R. In the simplest approximation it is assumed, based on simple molecular packing constraints (see Sec. 1.3.2), that the amphiphiles cannot organize into vesicles of radius R (size s) smaller than some critical value R_c (size s_c), and that $\tilde{\mu}_s^o$ is constant for $s \geq s_c$. Then, clearly, entropy considerations imply that most vesicles will be of radius R_c. (From (1.22) or (1.26) we see that if $\tilde{\mu}_s^o$ is constant then X_s/s decreases exponentially with s.) A rather different approximation corresponds to assuming that $\tilde{\mu}_s^o \sim k/R^2$ with k denoting the bilayer's bending constant (Sec. 1.3.4). Then, assuming that the average area per molecule is the same for all vesicles, it follows that $s \sim R^2$ and hence $\tilde{\mu}_s^o \sim 1/s$ or $\mu_s^o = \textit{constant}$. This model yields $X_s = As[X_1 \exp(\beta\mu_1^o)]^s = As\exp(s\beta\mu)$, with $A = \exp(-\beta\mu_s^o) = \textit{constant}$ (cf. (1.22) and (1.26)). This distribution is considerably broader than the one corresponding to $\tilde{\mu}_s^o = \textit{constant}$. It can be improved by including the (logarithmic) dependence of the elastic constant on vesicle size, which also improves the agreement with experiment [83].

Finally, we note that so far we have only considered "pure", that is, single component, aggregates. Generally speaking, the formation and growth of *mixed aggregates* are governed by the same principles prevailing in solutions of pure aggregates [88–90]. However, additional complexities (and possibilities) arise, because of the new thermodynamic degree of freedom corresponding to amphiphile composition. Consider, for example, a solution of two amphiphiles A and B, each of which separately prefers the formation of aggregates of different geometry. Suppose, for example, that A prefers a cylindrical environment whereas B has a slight preference for a spherical geometry. Because of the natural thermodynamic tendency for

mixing, the two amphiphiles will tend to form mixed aggregates (although the formation of separate A and B aggregates is also a possibility). Most likely, the mixed aggregates formed in this system will be rod-like micelles in which the B molecules will tend to concentrate in the spherical ends, while the A's prefer the cylindrical body. In other words, the molecular compositions in the two regions of the micelle can be different. (This corresponds to minimizing the packing free energy; see Sec. 1.3.) Furthermore, the overall A/B ratio in a micelle may depend on its size. These qualitative notions can be cast in standard statistical thermodynamic terms, and although the mathematical procedure is more involved than in Sec. 1.2.4, the derivations are rather straightforward. For example, in the case of a mixed system of rod-like micelles it has been shown that $\langle s \rangle_w \sim X^{2/5}$ as compared to the $\langle s \rangle_w \sim X^{1/2}$ behavior for pure aggregates [88]. Surfactant segregation ("repartitioning") into different regions of a micelle has been observed in several experimental studies [91–93]. However, the variation of $\langle s \rangle_w$ according to $X^{2/5}$ still awaits experimental verification.

Another example of an interesting and extensively studied class of systems corresponds to binary mixtures of phospholipids (e.g., lecithin) and 'detergents' (e.g., bile salts) and ternary systems including cholesterol as well. Here, the stable aggregation geometry as well as the micellar size depends on overall composition. For example, below a certain bile salt/lecithin ratio a dilute solution of these molecules consists of stable mixed vesicles. However, above this ratio the vesicular form becomes unstable and the solution (becomes transparent and) contains mixed *micelles* instead. It is believed that these micelles are composed of a disk-like (bilayer) body containing mainly lecithin, which is surrounded by a bile-salt rim [92].

There are many other examples of multi-component amphiphilic systems exhibiting diverse structures in dilute solutions. Even richer polymorphism is found in concentrated solutions, as is amply demonstrated in Sec. 1.4 and in some of the other chapters in this volume.

1.2.6 The Aggregate's Partition Function: Rotation-Translation Contributions

The basic premise of the phenomenological approach to micellar growth described in the previous sections is that the standard chemical potential of an s-aggregate, μ_s^o, is a weighted sum of contributions from the different regions of the aggregate, as expressed generally in (1.33) or, for simple geometries by (1.34) and (1.35). In the standard treatments of micellar growth, such expressions are usually postulated, without attempting to justify or assess their validity. This may be related to the common interpretation of μ_s^o as "the internal free energy of the aggregate", in analogy to the free energy of a (stationary) macroscopic system. Eq. (1.33) corresponds to extending this analogy to macroscopic systems composed of several subsystems g.

For *finite* aggregates some caution is required in identifying the degrees of freedom contributing to the free energy represented by μ_s^o. To this end we now return to the basic statistical thermodynamic relation (1.12) (or (1.17))

$$\mu_s^o = -kT \ln(q_s/V) \tag{1.50}$$

and examine to what extent (1.33) is consistent with the general expression for the aggregate's partition function. (Note that μ_s^o in (1.50) is in fact $\mu_s^{o,\rho}$ which differs from μ_s^o of (1.17) by an additive constant.) As stressed at the very beginning of Sec. 1.2.1, a rigorous calculation of q_s is hopeless, because micellar aggregates are such complex systems. Nevertheless, one could expect that the more modest goal of evaluating the s dependence of q_s is, perhaps, more feasible. We shall see, however, that even this goal involves some highly nontrivial difficulties.

Let $f = t+r+c$ denote the number of degrees of freedom (d.f.) of a single amphiphile. For a monomer in solution, $t = 3$ is the number of translational (center of mass) degrees of freedom, $r = 3$ is the number of overall rotations of the molecule, and c is the number of internal or conformational degrees of freedom. Consider, for example, a simple amphiphile of the form P–$(CH_2)_{n-1}$–CH_3, with P denoting the polar head group, which for simplicity will be assumed to be structureless. It is well known that the flexibility of these molecules is due, almost exclusively, to internal rotations around C–C bonds (see Sec. 1.3.3). All other modes, such as C–H and C–C stretches and C–C–C, C–C–H or H–C–H bends can be treated as frozen. (In fact, all we need to assume in order to ignore these modes in the present discussion is to establish that they are not affected by the state of aggregation of the amphiphiles.) Thus, the number of relevant internal degrees of freedom is $c = n - 1$, corresponding to the number of internal rotations around the backbone (non-terminal) C–C bonds.

In a micelle, due to the high packing density and the strong interactions between neighboring molecules, all f degrees of freedom of a given molecule are strongly coupled to each other, as well as to those of the other molecules. The translational motions are strongly hindered, and are more adequately described as vibrations, with occasional small jumps of the center of mass (or head-group) of the molecule. Without specifying the exact character of these motions, we shall assume that they can be treated classically. (This assumption may not be valid, for example, for the crystalline states of lipid bilayers.) The overall molecular rotations are even more strongly hindered. In fact, in the aggregate an overall rotation of the amphiphile, with a given (frozen) conformation, is obviously impossible; any rotation must involve conformational changes of both the rotating chain itself and its neighbors. Thus, in the aggregate, it is more appropriate to describe the conformational state of a molecule by $c + r$ (rather than by c) degrees of freedom; c numbers specify the bond (e.g., trans/gauche) sequence $\mathbf{b} = b_1 \cdots b_c$ of the chain (with $\{b_i\}$ the successive dihedral angles), and $r = 3$

numbers specify the overall orientation of the chain, Ω, with respect to some fixed coordinate system. Here, and in Sec. 1.3, we shall refer to $\alpha \equiv \mathrm{b}, \Omega$ as the conformational state of the molecule. For concreteness let us assume that the corresponding $r + c$ d.f. are non-classical.

Based on the division of the $s \cdot f$ d.f. of the aggregate into 3s (hindered) classical translations and $(f-3)s$ conformational d.f., the aggregate's partition function is given by

$$q_s = \frac{1}{h^{3s} s!} \int dp^{3s} \int dr^{3s} \sum_{\alpha^s} \exp\left[-\beta H\left(p^{3s}, r^{3s}, \alpha^s\right)\right] \tag{1.51}$$

where h is Planck's constant and $\beta = 1/kT$. r^{3s} and p^{3s} refer to the $3s$ position coordinates and $3s$ conjugate momenta of the s molecules, and α^s to their chain conformations. The Hamiltonian can be separated into kinetic and potential energy contributions

$$H = \sum_{i=1}^{3s} p_i^2/2m + W\left(r^{3s}, \alpha^s\right) \tag{1.52}$$

The potential energy W includes all the intermolecular interaction potentials, the internal (conformational) chain energies, and the interactions between the aggregated molecules and the surrounding solvent. With H given by (1.52) the integration over momenta in (1.51) is immediate, yielding

$$q_s = \frac{Z_s}{\lambda^{3s}} \tag{1.53}$$

with $\lambda = (h^2/2\pi mkT)^{1/2}$ denoting the de Broglie wavelength of a surfactant molecule, m being the amphiphile's mass. Z_s is the aggregate's configurational integral

$$Z_s = \frac{1}{s!} \int dr^{3s} \sum_{\alpha^s} \exp\left[-\beta W\left(r^{3s}, \alpha^s\right)\right] \tag{1.54}$$

Substituting (1.53) into (1.50) we can express the standard chemical potential as a sum of momentum and configurational terms

$$\begin{aligned} \mu_s^o &= \mu_s^{o,m} + \mu_s^{o,c} \\ &= skT \ln \lambda^3 - kT \ln(Z_s/V) \end{aligned} \tag{1.55}$$

Recall from (1.26) that the micellar size distribution X_s is governed by the s-dependence of $\mu_s^o - s\mu_1^o = s(\tilde{\mu}_s^o - \mu_1^o)$ or, equally, by $\tilde{\mu}_s^o - \tilde{\mu}_r^o$ with r denoting an arbitrary size. Since $\tilde{\mu}_s^{o,m} = kT \ln \lambda^3$ is a constant, it is clear that the *momentum* term in (1.55) is of no consequence for the micellar size distribution [53]. More explicitly, from (1.26) and (1.55), we see that X_s,

$$X_s = sX_1^s \frac{(Z_s/V)}{(Z_1/V)^s} \tag{1.56}$$

depends only on the configurational factors in the aggregate's partition function. Note also that the momentum terms in μ_s^o satisfy trivially the phenomenological expression $\mu_s^o = \sum s_g \tilde{\mu}_g^o$, cf. (1.33). (This follows immediately from the fact that we can define $kT \ln \lambda^3 \equiv \tilde{\mu}_g^{o,m} = constant$, hence $\tilde{\mu}_s^{o,m} = skT \ln \lambda^3 = \sum s_g \tilde{\mu}_g^{o,m}$.) Thus, not only X_s but also the validity of (1.33) depends only on the configurational part of μ_s^o.

For a given α^S, the potential energy $W(r^{3S}, \alpha^S)$ can be expressed as a function of $3(s-1)$ relative position coordinates $\mathbf{r}_i - \mathbf{r}_j$, or in terms of $3(s-1)$ (independent) coordinates measured with respect to the aggregate's center of mass. Accordingly, the remaining three coordinates may be chosen to represent a particular ("reference") particle, or the center of mass. Integrating over these coordinates in (1.54) yields a factor of V, implying that Z_s/V is volume independent. Note further that the factor V extracted from Z_s is the configurational integral associated with the translational motion of the aggregate as a whole. Accordingly, Z_s/V can be interpreted as the configurational integral of an *immobile* aggregate. More precisely, this corresponds to a non-translating aggregate because there is no restriction on its overall rotational motions. For an aggregate with well defined geometry, g, one can always separate three (Euler) angles, specifying its overall orientation in space [42–45]. Since W_s is independent of these angles, an additional factor of $8\pi^2$, corresponding to the integral over the three angles, can be extracted from Z_s. Thus, $Z_s^o = Z_s/8\pi^2 V$ or, see (1.54),

$$Z_s^o = \frac{1}{8\pi^2 V s!} \int dr^{3S} \sum_{\alpha^S} \exp\left[-\beta W\left(r^{3S}, \alpha^S; g\right)\right] \qquad (1.57)$$

can be interpreted as the configurational integral of a completely stationary (i.e., non-translating and non-rotating) aggregate. The symbol g in $W(r^{3S}, \alpha^S; g)$ is meant to emphasize that the integral in (1.57) includes only those configurations corresponding to a stationary aggregate of a well-defined geometry g.

From the discussion above, it follows that $\mu_s^{o,c} = -kT \ln Z^o$ is the (configuration part of the Helmholtz) free energy of a stationary aggregate. In the limit of a macroscopic aggregate ($s \to \infty$) of a single basic geometry g, $\mu_s^{o,c}$ becomes an extensive thermodynamic property and hence $\mu_s^{o,c}/s \to \tilde{\mu}_g^{o,c} = constant$. Similarly, for an aggregate comprising *several* "macroscopic regions" g we expect $\mu_s^{o,c} \to \sum s_g \tilde{\mu}_g^{o,c}$, as suggested by the phenomenological representation (1.33). Thus, for large aggregates (1.33) is certainly an adequate expression for μ_s^o. Whether (1.33) is equally appropriate for small micelles is not as obvious, and requires detailed analysis of Z_s.

An exact calculation of Z_s remains beyond our scope. But even the more qualitative question regarding the s dependence of Z_s for finite aggregates is highly non-trivial. For example, it can be shown that the transformation of dr^{3S} from laboratory to center-of-mass coordinates involves a Jacobian containing a factor s^3 [44]. Additional s^k factors arise from the separation

of the overall rotational motion (see below). These factors in Z_s suggest that μ_s^o contains, in addition to terms varying linearly with s, also terms proportional to $\ln s$. The $\ln s$ terms become negligible as $s \to \infty$, but for finite s their inclusion in μ_s^o can significantly affect the calculation of X_s [54]. It should be stressed, however, that it is not clear that the s^k factors resulting from coordinate and angle transformations account for the entire s-dependence of Z_s. Very similar questions arise in nucleation theory [42–45], where considerable controversy still exists regarding the most consistent way to separate the external motions of a cluster from the internal motions of its constituent particles.

In (1.53), based on (1.52) and (1.51), we have expressed q_s as a product of configurational and momentum factors. But this is not the only reasonable representation of q_s. Another one corresponds to a factorization of q_s into a product of translational, rotational and internal partition functions,

$$q_s = q_s^T q_s^R q_s^I \,. \tag{1.58}$$

This form has been adopted by a number of authors in their analyses of amphiphile self-assembly [48–52,54]. We shall briefly consider (1.58) below, because it clearly demonstrates the (possible) appearance of s^k factors in q_s. Eq. (1.58) represents a common factorization of molecular partition functions; namely, for diatomic or polyatomic molecules, it is always possible to separate out the center-of-mass translation [94]. Neglecting vibration-rotation coupling, one can also separate a rotational partition function, so that q_s^I corresponds to a vibrational partition function. Similarly, it can be shown that (1.58) is valid for any aggregate with well-defined center-of-mass and moments of inertia (i.e., well- defined shape and mass distribution) [42,43]. Accordingly, we can write

$$\mu_s^o = \mu_s^{o,TR} + \mu_s^{o,I} \tag{1.59}$$

with

$$\mu_s^{o,TR} = -kT \ln \left(q_s^T q_s^R / V \right) \tag{1.60}$$

and

$$\mu_s^{o,I} = -kT \ln q_s^I \tag{1.61}$$

The translation-rotation partition function $q_s^T q_s^R = q_s^{TR}$ involves six degrees of freedom; three corresponding to center of mass translation and three to the overall rotations of the aggregate when regarded as a rigid body. Thus, the internal partition function involves $3s - 6$ internal position and $3s - 6$ internal momentum coordinates, defined relative to an aggregate-fixed system of coordinates. Formally, q_s^I can be expressed as

$$q_s^I = \frac{1}{h^{3s-6} s!} \int dp^{3s-6} \int dr^{3s-6} \sum_{\alpha^s} \exp \left[-\beta H_I \left(p^{3s-6}, r^{3s-6}, \alpha^{3s} \right) \right] \tag{1.62}$$

The s-dependence of this quantity is extremely complicated and generally unknown except in highly idealized cases. As noted already with respect to Z_s there are, for example, s-dependent factors associated with the Jacobian of the transformation from the laboratory to the aggregate-fixed coordinate system. (Also, the $1/s!$ factor can be modified, as "part of it" should be absorbed into the symmetry numbers of the rotational partition function.)

On the other hand, the translational-rotational factors in (1.58) are simple. The translational partition function is $q_s^T = V/\Lambda_s^3$, with $\Lambda_s = \lambda/s^{1/2} = (h^2/2\pi smkT)^{1/2}$ denoting the deBroglie wavelength of the s-mer. The rotational partition function is given by $q_s^R = 8\pi^2/(\Lambda_{rot,s})^3$ with $\Lambda_{rot,s} = (h^2/2\pi I_s kT)^{1/2}$, I_s being the geometric mean of the aggregate's three moments of inertia, e.g., for rod-like micelles $I_s \sim s^{7/2}$. Thus for rods, say, $\mu_s^{o,TR}$ includes a $-5\ln s$ term ($5 = 3/2 + 7/2$). Now, if we assume that the separation $\mu_s^o = \sum s_g \tilde{\mu}_g^o$ should be applied to the internal free energy part only ($\mu_s^{o,I}$) in (1.59), then obviously μ_s^o will contain $\ln s$ contributions. E.g., for rods, it is easy to see that, instead of $\mu_s^o = s\tilde{\mu}_\infty^o + \delta kT$ (set $d = 1$ in (1.35)) we get $\mu_s^o = s\tilde{\mu}_\infty^o + (\delta - 5\ln s)kT$. Using this expression for μ_s^o, one finds a slower than $X^{1/2}$ increase of $\langle s\rangle$ with total concentration [54], which can be attributed to the fact that the translation-rotation entropy decreases with $\langle s\rangle$ and thus resists growth.

In the classical limit, when all the $3s$ degrees of freedom corresponding to molecular translations are classical, q_s is given generally by (1.51). In this limit the two representations (1.53) and (1.58) are equivalent in principle, provided the aggregate structure is consistently defined. (This sets constraints on coordinate integrations in the calculation of partition functions.) For dimers ($s = 2$) held together by a harmonic potential, this can be rigorously shown, provided the dimer is "tight", so that the vibrational amplitude is small compared to the distance between the two particles. The generalization to larger s-clusters, even simple ones like a linear array of "atoms" bound by harmonic restoring forces, is highly non-trivial. Thus, although we recognize that (in the classical limit) the two schemes (1.53) and (1.58) are equivalent, we cannot evaluate the exact s-dependence of q_s, q_s^I or Z_s. Clearly, both $\mu_s^{o,c} := -kT\ln Z_s^o$ and $\mu_s^{o,I} = -kT\ln q_s^I$ represent "internal free energies." Since we are equally ignorant about their exact s-dependence (except in one case—see below), the phenomenological expression may be arbitrarily applied to either $\mu_s^{o,c}$ or $\mu_s^{o,I}$. The only difference is that in the second case $\mu_s^o = \mu_s^{o,I} + \mu_s^{o,TR}$ will contain the $\ln s$ terms mentioned above. In the asymptotic ($s \to \infty$) limit, the difference disappears, but for finite aggregates it may affect the calculated size distribution.

It should be noted that there is one limiting, albeit somewhat hypothetical regime, where (1.58) is exact, whereas (1.53) is totally inadequate. This is the case of "rigid" (or solid) aggregates, i.e., aggregates in which all the intermolecular distances are fixed. Of course, in this case only the external rotations and translations (i.e., 6 degrees of freedom) can be treated as

classical. (Hence (1.51) is not applicable.) In this case the internal free energy $-kT \ln q^I$ is simply the internal energy of the aggregate, which can be expressed as a sum of contributions from different microenvironments, i.e., $\sum s_g \tilde{\epsilon}_g$, with $\tilde{\epsilon}_g$ denoting the energy per molecule in environment g. As a simple (idealized) example, suppose that a rod-like micelle is a rigid linear string of s beads, held to each other by nearest neighbor attractive potentials. Then, of course, the internal energy is exactly $2\epsilon_1 + (s-2)\epsilon_2$, with ϵ_1 and ϵ_2 corresponding to the energies of the terminal and non- terminal beads, respectively.

General discussions of rotation/translation vs. internal contributions to the micelle size distributions are found in the literature as early as 1957, when Hoeve and Benson [48] considered a factorization of q_s, which is virtually identical to (1.58). They calculated q_s^o assuming a liquid-drop model of the micellar interior, in conjunction with an estimate of the surface free energy. Then they determined the size distribution along the lines prescribed in Sec. 1.2.4. This approach has been extended from the canonical to the constant pressure ensemble by Aranow [49]. A detailed statistical-thermodynamic analysis, discussing various representations, and considering (qualitatively) the connection to the phenomenological descriptions has been given by Wulf [50]. Poland and Scheraga have also explicitly separated out the "external" (translation and rotation) contributions from q_s, writing them as proportional to s^n, with $n = 3/2$ (from translation) $+5/2$ (from rotation) in the case of spheres [51]. (Note that the mean moment of inertia $I_s \sim (I_A I_B I_C)^{1/3}$ scales as $s^{5/2}$ for spherical aggregates.) These $s^{5/2}$ factors in q_s give rise to $\ln s$ terms in μ_s^o which are partially cancelled in the Poland- Scheraga theory by contributions of the same form from $\ln q_s^I$. This partial cancellation between "external" and "internal" contributions has been considered most systematically by Nagarajan and Ruckenstein [52], with a rather different set of approximations invoked to treat the micellar interior. But, clearly, the subtle questions raised in this section require a great deal of further consideration before any firm conclusions can be reached concerning the relevant s-dependence of standard chemical potentials in the phenomenological treatment of self-assembly.

1.3 Molecular Organization of Aggregates

In Sec. 1.2 we have elaborated upon the central role of μ_s^o in amphiphile self-assembly and micellar growth. In the phenomenological approach (see (1.33)) μ_s^o is expressed as a superposition of the $\tilde{\mu}_g^o$'s, with $\tilde{\mu}_g^o$ representing the free energy per molecule in a microenvironment characterized by a single geometry g. So far, however, we have not considered at all the *microscopic* aspects of these quantities, namely, their relation to molecular

parameters and intermolecular interactions. This is our goal in the present section. We shall describe several theoretical models for the structure and thermodynamics of amphiphilic aggregates, and examine their underlying assumptions from a statistical thermodynamic point of view.

The importance of molecular theories of amphiphilic aggregates extends beyond their implications for micellar growth. There are numerous systems in chemistry, biology and other fields where the *internal structure* and properties of these systems are of utmost importance. To mention one important issue, the conformational statistics of the phospholipid molecules constituting biological membranes play a crucial role in determining the fluidity, elasticity and stability of these systems. Thus, Sec. 1.3.3 is devoted to a discussion of chain packing and conformational statistics of amphiphiles in various microenvironments. Curvature elasticity of amphiphilic films is treated explicitly in Sec. 1.3.4. Beforehand, we consider in Sec. 1.3.1 the separation of head-group and chain (or, surface vs. bulk) contributions to the free energy. Simple yet instructive and useful models for the structure and relative stability of amphiphilic aggregates are the subject matter of Sec. 1.3.2.

1.3.1 Separation of Head and Tail Contributions

In this section we focus on the statistical-thermodynamic properties of amphiphiles packed in a microenvironment of well-defined geometry g. Specifically, the thermodynamic system of interest is an (immobile) aggregate, or portion thereof, containing s amphiphiles which (neglecting end effects) can be treated as equivalent particles. A large section of a long cylindrical micelle, a sheet of a planar bilayer, a spherical micelle or a spherical vesicle are typical examples.

Let $F(s,g,T)$ denote the configurational free energy of the system, with $f = F/s$ the free energy per molecule. We are interested in the *macroscopic* ($s \to \infty$) limit, where end effects are negligible and $f = f(g,T)$ is strictly intensive. (The $s \to \infty$ limit is clearly an idealization for small micelles or vesicles.) In this limit $f(g,T)$ is identical to the configurational part of $\tilde{\mu}_g^o$, as discussed in Sec. 1.2.6, i.e.,

$$f(g,T) \equiv \tilde{\mu}_g^{o,c} \tag{1.63}$$

Recall also that when $s \to \infty$ the various standard chemical potentials, e.g., $\tilde{\mu}_g^{o,c}, \tilde{\mu}_g^o, \mu_{s,g}^o/s$ or $\mu_s^{o,I}/s$, differ from each other by uninteresting additive constants. For notational convenience we shall use $f(g,T)$ rather than any of the above μ^o's.

As usual, F is related to a configurational integral Z,

$$F(s,g,T) = -kT \ln Z(s,g,T) \tag{1.64}$$

with

$$Z(s,g,T) = C \int dr^{3s} \sum_{\alpha^s} \exp\left[-\beta W\left(r^{3s}, \alpha^s; g\right)\right] . \qquad (1.65)$$

As in (1.54) W is the potential energy of the aggregate assuming that the surrounding solvent is a continuous medium, so that W is in fact a potential of mean force [94]. Note that $Z(s,g,T)$ corresponds to the $s \to \infty$ limit of Z_s^o in (1.57), which is the configurational integral of a stationary aggregate. Accordingly, we can identify C as $1/8\pi^2 V s!$. ($1/s!$ corrects for the overcounting of configurations implied by the (unrestricted) integration over the position coordinates of the (identical) molecules. The $1/8\pi^2 V$ factor cancels out after integrating over the center of mass coordinates and rotation angles of the aggregate.)

As emphasized in the previous section, the calculation of Z is practically impossible because of the great complexity of amphiphilic aggregates. The most detailed approaches to date involve computer simulations, mainly molecular dynamics studies of the kind already discussed in Sec. 1.1 [36–41,95–105]. However, as stressed there, even these studies involve many difficulties and must employ drastic simplifying assumptions, as well as rely on uncertain intermolecular potentials. Some interesting results derived from computer simulations have been described in Sec. 1.1, and others will be mentioned in Sec. 1.3.3 below. However, most of the following discussion will be devoted to simple, but general, phenomenological models (Sec. 1.3.2) and mean-field theories (Sec. 1.3.3) where the "standard picture of micelles" outlined in Sec. 1.1 serves as a basic premise.

According to the "standard picture" every aggregate is composed of two well-defined regimes:

1. A hydrophobic core containing the hydrocarbon tails, packed such that the monomer (chain segment) density is uniform and liquid-like.

2. A surface region containing the polar head-groups, surrounded by solvent molecules (including counter ions in the case of charged amphiphiles), see Fig. 1.6. The two regimes are separated by a well-defined interface. The area per head-group, a, at the hydrocarbon-water interface and the principal curvatures $\mathrm{c} = c_1, c_2$ of this interface fully specify the geometry of the aggregate, i.e., $g \equiv a, \mathrm{c}$.

In the above model the head-groups always see the same (rather smooth) hydrocarbon surface, regardless of the many-chain configuration α^s within the hydrophobic core. Thus, associating $r_1, \cdots, r_s$ in $W(r^{3s}, \alpha^s; g)$ with the head-group positions relative to the interface, we can write $W(r^{3s}, \alpha^s; g) = W_h(r^{3s}; g) + W_t(\alpha^s; r^{3s}, g)$. W_h accounts for all the contributions to W from the head-group (surface) region. That is, $W_h = W_{hh} + W_{hs} + W_{ht} + W_{st}$ includes, respectively, head-group/head-group, head-group/solvent, head-group/hydrocarbon (tail) and tail/solvent interactions. A simple approximation for W_{st}, which includes the interactions between the solvent and

those segments of the tails residing at the interface, would be $W_{st} = \gamma A$, with γ denoting the (effective) hydrocarbon-water interfacial tension and $A = sa$ being the total surface area. The geometry ($g = a, \mathbf{c}$) dependence of W_h enters mainly through its dependence on a, the $\mathbf{c}$ dependence being weaker.

The tail term W_t accounts for all the interactions between chain segments inside the hydrophobic core. In Sec 1.3.3 we show that W_t, which determines the probabilities $P(\alpha^S)$ of the various chain configurations α^S, depends strongly on the aggregation geometry, g. On the other hand, the dependence of W_t on head-group positions, r^{3S}, is weak. Because of head-tail connectivity the statistical weights of the α^S are correlated with r^{3S}. Imagine, however, that the head-groups were clamped at some fixed lattice points corresponding to their equilibrium positions at the hydrocarbon water-interface. Then r^{3S} is fully specified by the geometry $g = a, \mathbf{c}$ of the interface, implying $W_t = W_t(\alpha^S; g)$. Similarly, averaging over r^{3S} would also yield $W_t = W_t(\alpha^S; g)$. Since only small deviations from this behavior are expected when the head-groups are fluctuating around the equilibrium positions, we can safely write

$$W(r^{3S}, \alpha^S; g) = W_h(r^{3S}; g) + W_t(\alpha^S; g) \tag{1.66}$$

It follows from this decomposition that (cf. 1.65)

$$Z(s, g, T) = Z_h(s, g, T) Z_t(s, g, T) \tag{1.67}$$

with

$$Z_h(s, g, T) = C \int dr^{3S} \exp\left[-\beta W_h\left(r^{3S}; g\right)\right] \tag{1.68}$$

$$Z_t(s, g, T) = \sum_{\alpha^S} \exp\left[-\beta W_t(\alpha^S; g)\right] \tag{1.69}$$

From (1.67) we see that the aggregate's free energy is a sum of head and tail contributions, $F = F_h + F_t$ with $F_h = -kT \ln Z_h$ and $F_t = -kT \ln Z_t$. Similarly, $f = F/s$ is also a sum of head and tail terms

$$f(g) = f_h(g) + f_t(g) \tag{1.70}$$

with both $f_h = F_h/s$ and $f_t = F_t/s$ depending on the aggregation geometry g.

In the next section we describe a phenomenological theory of $f(g)$. The term "phenomenological" used here refers to a theory which, based on some basic physical principles and assumptions, postulates a certain functional form for the free energy ($f(g)$ in our case). In other words, phenomenological theories circumvent the difficulties associated with direct calculation of partition functions. Quite often in complex systems the evaluation of partition functions involves so many approximations and assumptions that more

physical insights are gained from phenomenological models. Nevertheless, in Sec 1.3.3 we shall describe a mean-field theory for $f_t(g)$ which corresponds to an approximate evaluation of Z_t and which provides considerable insight into the microscopics of chain packing statistics in hydrophobic environments.

1.3.2 Hydrocarbon Droplet Models

Two phenomenological models for $f(g)$ have largely dominated the discussion of amphiphile packing and micellar size and shape in recent years. These models, one due to Tanford [30] and the other to Israelachvili, Mitchell and Ninham (IMN) [31] share many common features but differ markedly in some important aspects. Consistent with the "standard picture of the micelle", both theories treat the hydrophobic core as a liquid hydrocarbon droplet. More specifically, it is assumed that the hydrocarbon tails in the hydrophobic regions of the aggregates behave like the corresponding chains in the bulk liquid alkane. Following this assumption, both models assume that the tail term in (1.70) is a constant, independent of the micellar geometry, i.e.,

$$f_t(g) = f_t = constant\ . \tag{1.71}$$

Furthermore, in both the Tanford and the IMN models, the dependence of $f_h(g) = f_h(a, \mathbf{c})$ on the area per head-group a is evaluated in terms of the "opposing forces" (see Sec. 1.3.2.2 below). The difference between the two approaches is manifested in the different criteria for determining the optimal aggregation geometry, i.e., the one corresponding to minimal $f(g)$.

In this section we present, in a common language, the basic concepts underlying these different phenomenological models, and comment critically on the various approximations involved. We shall mainly follow the IMN approach which provides a simple and elegant ("first order") scheme for determining the optimal geometry. The relation to Tanford's model will be mentioned at the appropriate junctures.

1.3.2.1 Geometric packing constraints and surface-volume relations

Let l denote the length of a fully extended amphiphile chain. l scales linearly with the number of chain segments, n; e.g., for simple alkyl tails, $-(CH_2)_{n-1}-CH_3$, the length of an all-trans chain is [30] $l(\text{Å}) \approx 1.5+1.27n$. The volume per chain, v, as measured in the bulk liquid alkane, also scales with n, e.g., for alkyl chains [30] $v(\text{Å}^3) \approx 27.5 + 27n$. Since there are no holes in the hydrophobic core, its smallest dimension must be smaller than $2l$. For instance, in a spherical micelle the radius R cannot exceed the length of a fully stretched chain, i.e., $R \leq l$. The same constraint applies to the radius R of (the circular cross section of) a cylindrical aggregate. Similarly, in planar bilayers $R \leq l$, where $R \equiv D/2$ is the half-thickness of

the bilayer. In the following discussion we shall continue to consider $g =$ *sphere, cylinder* and *bilayer*, the three "basic" geometries.

For a spherical micelle of radius R which contains s amphiphiles, the total volume of the hydrophobic core is $V = (4/3)\pi R^3 = sv$, and its total surface area is $A = 4\pi R^2 = sa$, implying $a = 3v/R$. Similar considerations yield $a = 2v/R$ and $a = v/R$ for cylinders and planar bilayers, respectively. From the packing constraint $R \leq l$ it now follows that the areas per head-group in the three basic geometries must satisfy

$$a \geq a_{\min}(g) = i_g \left(\frac{v}{l}\right) \tag{1.72}$$

with $i_g = 1, 2$ and 3 for spheres, cylinders and bilayers, respectively. (Note $i_g = 3 - d$ with d denoting the dimensionality of the aggregate, cf. Sec. 1.2.4.)

As a numerical example illustrating the significance of (1.72) consider, say, a 12-carbon tail such as in SDS. Setting $n = 12$ in the above expressions for the volume per chain and all-trans length, we find for this molecule $v \approx 350\text{Å}^3$ and $l \approx 16.7\text{Å}$. (According to Tanford [30], the first CH_2 group of the tail resides mainly outside the hydrophobic core, so that $v \approx 320\text{Å}^3$ and $l \approx 15.5\text{Å}$, but we ignore these subtleties here.) These values imply that the minimal area per SDS head-group (see (1.72)) in a spherical micelle is $a \approx 63\text{Å}^2$, and the corresponding lower limits for cylinders and bilayers are 42Å^2 and 21Å^2, respectively. The last value, 21Å^2, is indeed close to the common estimate of the minimal cross sectional area of (all-trans) chains in bilayers and monolayers (see Chap. 12).

This example has demonstrated that SDS chains, for example, can be packed into different types of aggregates, provided the area per molecule, a, complies with (1.72). We now turn to consider which of these geometries is the *optimal* one.

1.3.2.2 The opposing forces

In the phenomenological models f is expressed as an explicit function of a, whereas its dependence on curvature $\mathbf{c}$ centers only as a correction. Thus, for the present discussion we shall assume $f(g) = f(a, \mathbf{c}) = f(a)$. (We treat curvature elasticity of amphiphile *films*, i.e., the $\mathbf{c}$ dependence of f, in Sec. 1.3.4.) Both IMN and Tanford express $f(a)$ as

$$\begin{aligned} f(a) &= f_h(a) + f_t \\ &= \gamma a + \frac{\kappa}{a} + f_t \end{aligned} \tag{1.73}$$

with f_t representing the constant tail contribution, as assumed in (1.71).

The first two terms in the second equality correspond to one of the simplest representations of f_h in terms of the "opposing forces" [30–33]. The first term, γa, is the interfacial free energy associated with hydrocarbon-water contact, with γ denoting the effective surface tension. (Recall that

γa is related to the W_{st} term of W_h, as described in Sec. 1.3.1.) Since γa increases with a, this term tends to reduce the area per head group, and in this sense corresponds to an attractive interaction between head-groups. On the other hand, as a decreases, head-group–head-group repulsion increases due to electrostatic or excluded volume interactions, or both. The second term in (1.73), κ/a, is the leading term of the repulsive potential (per molecule) in a system of ionic or zwitterionic head-groups. The constant κ can be estimated from simple models, or empirically (together with γ) from experimental data [30–33,53]. Many authors have studied the electrostatic free energy in the interfacial region in a more quantitative fashion [30,33,55,106–111] based either on solving the Poisson-Boltzmann equation [55,106–108] or via computer simulations [111]. For the qualitative discussion here it suffices to represent these effects by the simple form κ/a. If the repulsion is predominantly steric (excluded area), other representations may be more adequate than κ/a, e.g., a van der Waals-like repulsion $\ln[1/(a-\hat{a})]$, with $\hat{a}$ denoting the excluded area per head-group [112].

Let a_h denote the area per head-group which minimizes $f_h(a)$. From (1.73) we find that $a_h = \sqrt{(\kappa/\gamma)}$. The parameters κ and (to a lesser extent) γ depend on the nature of the head-groups and the properties of the surrounding solution (e.g., the ionic strength). Thus a_h is also determined by the properties of the head-group and the solution, but is independent of the amphiphile tail. Substituting $\kappa = \gamma a_h^2$ into (1.73), we get

$$f(a) = 2\gamma a_h + \frac{\gamma}{a}(a - a_h)^2 + f_t \,. \tag{1.74}$$

The second term here accounts for the excess free energy associated with packing the amphiphile with an area per head-group a different from the optimal area a_h. The common estimates of γ range between (25–50) erg/cm^2 which, at room temperature, correspond to $\approx (0.05 - 0.1)kT/\text{Å}^2$. Thus, for example, if $a_h = 30\text{Å}^2, a = 40\text{Å}^2$ and $\gamma = 0.05kT/\text{Å}^2$ we find that the excess free energy is $\approx 0.1kT$ per molecule.

1.3.2.3 The optimal aggregation geometry

The physical content of the assumption (1.71) is that the chains can adjust conformationally so as to comply with any packing geometry, *at no free energy cost*. The accuracy of this approximation is discussed in more detail below (cf. Sec. 1.3.3). Subject to this approximation, $a = a_h$ minimizes not only $f_h(a)$, but $f(a) = f_h(a) + f_t$ as well. Thus, in the IMN model a_h represents the *optimal* area per head-group.

The next, and very crucial, step in the IMN model is to assume that in all aggregation geometries the area per amphiphile head-group is always $a = a_h$, thus ensuring that $f(a)$ is *always* at a minimum ($= 2\gamma a_h + f_t$). But the condition $a = a_h$ can be satisfied by more than one aggregation geometry, and is thus not sufficient to determine the optimal geometry. For example, if for a given amphiphile $a_h \geq 3(v/l)$, then according to (1.72) the

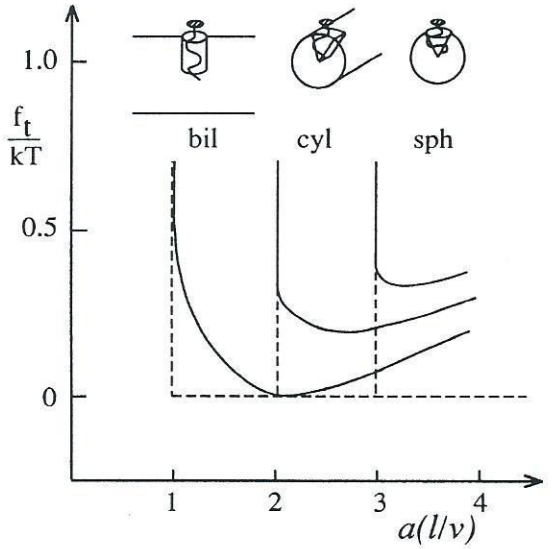

FIGURE 1.9. The packing (conformational) free energy of amphiphile tails in the three basic aggregation geometries, as a function of the area per head-group. The dashed lines, indicating a constant value for f_t for all values of a which are consistent with the molecular packing constraints, correspond to the hydrocarbon-droplet assumption (see text). The full lines represent typical results obtained from more detailed theories of chain packing in the different microenvironments [115, 116, 120-122].

molecules can be packed into spheres, cylinders or planar bilayers at the same free energy cost: $f(a = a_h)$. According to IMN the amphiphiles will preferentially organize in spherical micelles, because for a given total concentration, this arrangement maximizes the "mixing" (disperson) entropy of the system—as discussed in Sec. 1.2.2. If, however, $3(v/l) > a_h > 2(v/l)$, spherical micelles are unstable because they require $a \geq 3(v/l) > a_h$. In this case, for similar reasons as above (i.e., maximum dispersion entropy), cylindrical micelles are the preferred micellar geometry. Finally, if $2(v/l) > a_h \geq (v/l)$, a planar bilayer is the only stable aggregation geometry (among the three basic shapes considered). These conclusions are summarized schematically in Fig. 1.9. Figure 1.9 displays also the dependence of f on a as derived from mean field theories which take into account the variation of f_t with a, i.e., without assuming $f_t(a) = \textit{constant}$ (see Sec. 1.3.3.) The differences between the minima of the $f(a)$ curves corresponding to the different aggregation geometries are typically of the order of $(0.1 - 0.5)kT$, i.e., of the same order of magnitude implied by (1.74) for $a - a_h \approx 10\text{Å}^2$.

We conclude this section with a comment on Tanford's interpretation [30] of the (hydrocarbon droplet) assumption $f_t = constant$, which differs diametrically from that of IMN. He assumes that the chains preserve the same degree of conformational freedom in all the aggregates. In particular, he assumes that, as in bulk hydrocarbon liquids, the mean end-to-end chain length, b, obeys $b \approx 0.75l$ in *all* aggregation geometries. Combining this requirement with simple geometric considerations (of the type leading to (1.72)), one can calculate the values of a corresponding to any aggregation geometry (spheres, oblate or prolate micelles, etc.). Tanford then uses (1.73) to calculate $f(a)$ for each possible geometry, and the optimal one is chosen to be the one corresponding to the minimal value of $f(a)$. In general, the average a corresponding to the stable geometry is different from a_h, i.e., a_h does not play any significant role in Tanford's model.

1.3.3 Chain Packing Statistics

All the information about chain organization in an aggregate of geometry g (or portion thereof) is contained in the many-chain distribution function

$$P(\alpha_1, \alpha_2, \ldots, \alpha_s) = \frac{1}{Z_t} \exp\left[-\beta W_t(\alpha^s, g)\right] \tag{1.75}$$

which gives the probability of finding the s chains in configuration $\alpha_1, \alpha_2 \cdots \alpha_s = \alpha^s$. $Z_t = Z_t(s, g, T)$ is the configurational integral (1.69). Thermodynamic functions can also be expressed in terms of $P(\alpha^s)$. In particular, the configurational free energy is given by

$$\begin{aligned} F_t &= E_t - TS_t = -kT \ln Z_t \\ &= \sum_{\alpha^s} P(\alpha^s) W_t(\alpha^s) + kT \sum_{\alpha^s} P(\alpha^s) \ln P(\alpha^s) \end{aligned} \tag{1.76}$$

with $E_t = \sum_{\alpha^s} P(\alpha^s) W_t(\alpha^s) = kT^2(\partial \ln Z_t/\partial T)$ and $S_t = -k \sum P(\alpha^s) \ln P(\alpha^s) = k \ln Z_t + kT(\partial \ln Z_t/\partial T)$ denoting the system's energy and entropy, respectively.

Owing to the great complexity of amphiphilic aggregates, computer simulations appear to be the only reasonable approach for calculating many-chain properties related to $P(\alpha^s)$. However, these studies encounter various kinds of technical difficulties, as noted already in previous sections. On the other hand, it should be realized that most of the experimental measurements of chain conformational statistics in micelles and bilayers involve single chain properties such as bond order parameter profiles or segment spatial distributions. These properties are determined by the singlet probability distribution function (*pdf*) of chain conformations $P(\alpha)$, which gives the probability of finding a given chain in conformation α, regardless of (i.e., averaged over) the conformations of all other chains. The singlet probability of finding chain 1, for instance, in conformation $\alpha_1 = \alpha$

is given by

$$P(\alpha) = \sum_{\alpha_2,\cdots,\alpha_S} P(\alpha, \alpha_2, \cdots \alpha_S) \tag{1.77}$$

In addition to conformational properties, $P(\alpha)$ can be used to calculate, in the mean-field approximation, any thermodynamic function of interest (see below).

The calculation of $P(\alpha)$ and derivable conformational and thermodynamic properties is the central objective of the mean-field (or "single-chain") theories of chain packing in micelles and bilayers. Several authors, beginning with Marcelja's study of lipid chain packing and phase transitions in bilayers [113], have formulated such theories, differing from each other in various respects (e.g., lattice vs. non-lattice models) but also sharing some common important features (e.g., the assumption of uniform liquid-like hydrophobic core) [113–128]. The common and discrepant aspects of the various approaches have been critically analyzed elsewhere [121].

In the discussion below, we follow closely the approach described in [120–126]. Our goal is to describe the basic conformational and thermodynamic characteristics of chains packed in microenvironments of different geometries. Our treatment is based largely on the application of a simple explicit expression which we shall derive for $P(\alpha)$. Underlying our derivation are simple geometric packing considerations which will be discussed first.

1.3.3.1 Chain packing constraints

Figure 1.10 describes schematically a portion of the hydrophobic core of an aggregate containing s chains, originating from an interface of total area A. The local geometry $g = a, c_1, c_2$ is specified by the average area per molecule $a = A/s$ and the local curvatures $c_1 = 1/R_1$ and $c_2 = 1/R_2$, with R_1, R_2 denoting the principal radii of curvature. Let $a(x)$ denote the average cross sectional area available per chain at (normal) distance x from the interface. Using $c > 0$ for convex interfacial curvatures (viewed from the hydrophobic core), we have

$$a(x) = a\left[1 - (c_1 + c_2)x + c_1 c_2 x^2\right] \tag{1.78}$$

with $a = a(0)$. Thus, for planar interfaces ($c_1 = c_2 = 0$) such as in lipid bilayers or surfactant monolayers $a(x) = a = \textit{constant}$. In spherical micelles, where $c_1 = c_2 = 1/R$, the area diminishes rapidly towards the center: $a(x) = a(1 - x/R)^2$. For chains packed in cylindrical geometries ($c_1 = 1/R, c_2 = 0$) the area decreases linearly with the distance from the interface: $a(x) = a(1 - x/R)$. On the other hand, $a(x)$ *in*creases with x for chains packed in *concave* geometries such as the inner leaflet of a vesicle, the surface of a water-in-oil microemulsion droplet, or the cylinders constituting reversed hexagonal phases.

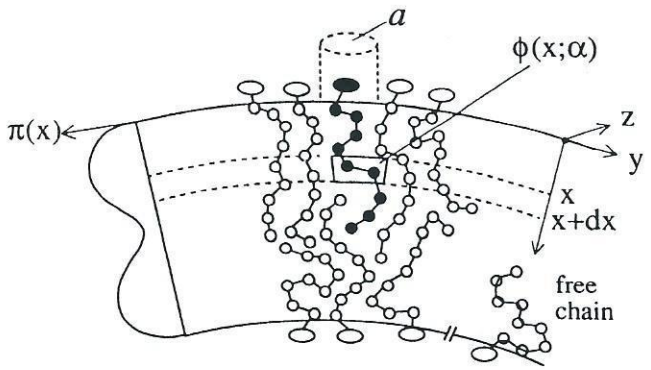

FIGURE 1.10. Schematic illustration of the origin of chain packing (uniform monomer density) constraints in the hydrophobic core. $\phi(x;\alpha)dx$ is the volume occupied by (or the number of monomers of) the 'central' chain within the layer $x, x+dx$ when the chain is in conformation α. $\pi(x)$ is the lateral pressure profile (see text). Also illustrated is a "free chain", i.e., one with no neighbors around and which is thus not subjected to packing constraints.

Let $\phi(x;\alpha)dx$ denote the volume taken up by a chain in conformation α, in the shell $x, x+dx$ of the hydrophobic core; see Fig. 1.10. More precisely, in our calculations we identify $\phi(x;\alpha)dx/\nu$ with the number of (centers of) segments of an α-chain within $x, x+dx$, where ν is the volume per chain segment in the bulk liquid hydrocarbon phase. Note that ϕ has dimensions of *area*. (For alkyl chains $\nu = \nu(CH_2) \approx 27\text{Å}^3$, except for the terminal CH_3 group which can be counted as two segments: $\nu(CH_3) \approx 2\nu(CH_2)$ [30].) Except for lipid chains in the crystalline ("gel") bilayer phase, which is not of interest here, $\rho_l = 1/\nu$ represents an upper limit to the monomer density in the hydrophobic regions of amphiphilic assemblies.

The local monomer density at distance x from the interface is $\rho(x) = \rho_l\langle\phi(x)\rangle/a(x)$ where $\langle\phi(x)\rangle = \sum P(\alpha)\phi(x;\alpha)$. Since $\rho(x) \le \rho_l = 1/\nu$ we get

$$\langle\phi(x)\rangle = \sum_{\alpha} P(\alpha)\phi(x;\alpha) \le a(x) \tag{1.79}$$

with the equality holding when the monomer density is uniform and liquid-like throughout the hydrophobic core. Note, however, that the condition of uniform density $\rho(x) = \rho = \textit{constant}$ is weaker than $\rho(x) = \rho_l$. ρ must satisfy $\rho = \rho_l(v/\hat{v})$, where $v = \int\langle\phi(x)\rangle dx = \int\phi(x;\alpha)dx$ is the chain's total volume, and $\hat{v} \equiv \int a(x)dx$ is the *available* volume per chain.

Following the discussion in Sec. 1.1, we shall assume that the condition of uniform monomer density applies to "compact" aggregates such as micelles

and lipid bilayers. An example of a "non-compact" system is a surfactant monolayer adsorbed at a water-air or water-oil interface [124]. We shall often refer to monolayers throughout this section, but our interest will be focussed on compact aggregates. We therefore rewrite (1.79) for the important case of uniform monomer density,

$$\langle \phi(x) \rangle = \sum_{\alpha} P(\alpha)\phi(x;\alpha) = a(x) \tag{1.80}$$

which represents a key mathematical constraint on the singlet *pdf* $P(\alpha)$.

The extension of (1.80) to mixed aggregates is straightforward, e.g., for binary aggregates containing chains of types A and B, in proportions X_A and $X_B = 1 - X_A$, respectively, we have

$$X_A \sum_{\alpha} P_A(\alpha)\phi_A(x;\alpha) + X_B \sum_{\beta} P_B(\beta)\phi_B(x;\beta) = a(x)\ , \tag{1.81}$$

with α and β representing the conformations of chains A and B, respectively. This condition is also applicable to hydrophobic cores which are packed by segments of chains originating from different interfaces, such as in lipid bilayers [122].

1.3.3.2 The singlet distribution

The potential energy $W_t(\alpha_1 \cdots, \alpha_s)$ in (1.75) and (1.76) is a sum of single (internal) chain energies $\epsilon(\alpha_i)$ and an intermolecular interaction potential $U(\alpha_1 \cdots, \alpha_s)$. The internal energies $\epsilon(\alpha)$ are easily calculated, e.g., in the rotational isomeric state model [129] (see below) and their contribution to $P(\alpha^S)$ and Z_t is simple. On the other hand, the effects of U are complicated, and their analysis requires a number of approximations.

Our first approximation is to separate u into two terms $U(\alpha^S) = U_{hc}(\alpha^S) + U_{att}$. The first term, $U_{hc}(\alpha^S) = \sum U_{hc}(\alpha_i, \alpha_j)$, is a sum of short range, or more specifically hard-core, repulsive interchain potentials. Thus, $u_{hc}(\alpha^S) = \infty$ for all configurations where (segments belonging to any) two chains or more overlap in space; otherwise, that is, for non-overlapping configurations, $U_{hc}(\alpha^S) = 0$. The second term, U_{att}, incorporates the long-range attractive potentials, and is assumed to be independent of $\alpha_1, \cdots, \alpha_S$ for chains packed at uniform monomer density. In other words, $U_{att} = su$ is regarded as a uniform attractive background, with u denoting the average "cohesive" energy per chain: for simplicity, we shall set $u = 0$. According to the above separation of $U(\alpha^S)$, the configurational properties are determined by the hard-core (excluded volume) repulsive potential $U_{hc}(\alpha^S)$. This approximation is inspired by a similar representation of U which underlies many theories of simple liquids whose structure is known to be dominated by the short range potential [130].

From the discussion above it follows that

$$W_t(\alpha^s) = \begin{cases} \sum_i \epsilon(\alpha_i), & \text{non-overlapping } \alpha^s \\ \infty, & \text{overlapping } \alpha^s \end{cases} \tag{1.82}$$

Thus, $P(\alpha^s) = 0$ for forbidden configurations, whereas for the allowed configurations $P(\alpha^s) \propto \exp[-\beta \sum \epsilon(\alpha_i)]$. Using the definition of E_t in (1.76) and of $P(\alpha)$ in (1.77), we find that (1.82) implies $E_t = \sum_i \sum_\alpha P(\alpha_i)\epsilon(\alpha_i) = s \sum_\alpha P(\alpha)\epsilon(\alpha) = s\langle\epsilon\rangle$. Thus, E_t becomes a simple sum of single chain energies. Clearly, (1.82) does not greatly simplify the calculation of Z_t, since exact counting of the allowed configurations remains an impossible task. However, it allows the derivation of a simple expression for $P(\alpha)$, as outlined next by two approaches.

(i) Mean-field approach

In this approach $P(\alpha^s)$ is expressed as a product of singlet *pdf*'s

$$P(\alpha_1, \cdots, \alpha_s) = P(\alpha_1) \cdots P(\alpha_s) \tag{1.83}$$

thus neglecting interchain correlations. Substituting (1.83) into (1.76) and using $E_t/s = \sum_\alpha P(\alpha)\epsilon(\alpha) = \langle\epsilon\rangle$ we find that the free energy per chain, $f_t = F_t/s$, is a simple functional of $P(\alpha)$,

$$f_t = \sum_\alpha P(\alpha)\epsilon(\alpha) + kT \sum_\alpha P(\alpha) \ln P(\alpha) \tag{1.84}$$

with $\langle\epsilon\rangle = \sum P(\alpha)\epsilon(\alpha)$ and $s_t = -k \sum P(\alpha) \ln P(\alpha)$ representing the energy and entropy contributions to f_t.

Eq. (1.84) is the exact free energy per chain only when (1.83) is valid, i.e., when the chains are independent, as would be the case if the chains are far apart from each other. Otherwise, (1.84) is an approximation to F/s even if $P(\alpha)$ is the exact singlet *pdf*. In general, $P(\alpha)$ is not known, but then f_t can be used as a variational free energy for deriving the best approximation for $P(\alpha)$: the desired *pdf* is the one which minimizes f_t subject to whichever constraints $P(\alpha)$ must fulfill.

Consider first the limit of non-interacting (or "free") amphiphiles corresponding to a system in which $a \gg a_f$, where a_f is the effective cross sectional area of a single, isolated, chain; see Fig. 1.10. In this case, $P(\alpha)$ is not subject to any constraint, except the normalization condition $\sum P(\alpha) = 1$. It can be shown that in this case f_t is minimized by [120]

$$P_f(\alpha) = \frac{1}{y_f} \exp[-\beta\epsilon(\alpha)] \,, \tag{1.85}$$

where $y_f = \sum_\alpha \exp[-\beta\epsilon(\alpha)]$ is the partition function of the free chain. Note that the conformational freedom of the free chain is limited by the existence of the hydrocarbon-water interface, which restricts the chain to

its hydrophobic side. Clearly, the number of allowed chain conformations, and consequently y_f, depend on the curvature of the interface, e.g., y_f is smaller for micelles (because of their convex interface), as compared to planar bilayers or inverted micelles. For micelles, bilayers and other compact aggregates, the free-chain is a hypothetical limiting case. In monolayers it represents the real chain in the limit of low surface density [124].

In the free chain limit $\langle \phi_f(x) \rangle \ll a(x)$, and (1.79) is trivially satisfied. This packing constraint becomes relevant only when a (recall that $a = a(x = 0)$) reduces to a value such that $\langle \phi_f(x) \rangle$ exceeds $a(x)$ for some x. (This may be taken as an operational definition of a_f.) At smaller a's excluded volume interactions become important, and the chains must be stretched, thus "sacrificing" conformational freedom, in order to satisfy the packing constraint. The packing constraints (1.79) for monolayers and (1.80) for compact liquid-like hydrophobic cores are the mathematical expression of (1.82) in the mean-field approach.

The minimization of f_t (see (1.84)) subject to (1.80) yields

$$P(\alpha) = \frac{1}{y} \exp\left[-\beta\epsilon(\alpha) - \beta \int \pi(x)\phi(x;\alpha)dx\right] \tag{1.86}$$

with

$$y = \sum_{\alpha} \exp\left[-\beta\epsilon(\alpha) - \beta \int \pi(x)\phi(x;\alpha)dx\right] . \tag{1.87}$$

Here $\pi(x)$ is a continuous set of Lagrange multipliers conjugate to the uniform packing constraint $\langle \pi(x) \rangle = a(x)$. $\pi(x)$ can be interpreted as the *lateral pressure* or (negative) stress profile; see Fig. 1.10. Indeed, $P(\alpha)$ is a generalized *isothermal-isobaric* probability distribution and y is the corresponding partition function. The integral $\int \pi(x)\phi(x;\alpha)dx$ is a generalized "PV" term, representing *the "mean-field" experienced by a "central" chain in conformation α due to the presence of close-by neighbor chains.* Consistent with this interpretation, we note that the free chain limit, (1.85), corresponds to $\pi(x) \equiv 0$. The integral $\int \pi(x)dx = \pi_t$ is the lateral pressure required to squeeze the chains so as to satisfy the packing constraint (1.80).

The numerical values of the $\pi(x)$ are determined by the packing constraints; namely, substituting (1.86) and (1.87) into (1.80), one gets, for every value of x

$$\sum_{\alpha} [\phi(x;\alpha) - a(x)] \exp\left[-\beta\epsilon(\alpha) - \beta \int \pi(x')\phi(x';\alpha)dx'\right] = 0 . \tag{1.88}$$

These "self-consistency" equations can be solved numerically for the $\pi(x)$, provided of course that the $\phi(x;\alpha)$ are known. A convenient solution procedure is to divide the hydrophobic core into L layers of thickness Δx. Correspondingly the integral in (1.88) (and similarly in (1.86) and (1.87)) transforms into a layer sum, and hence (1.88) becomes a set of L coupled

nonlinear equations, for $i = 1, \ldots, L$:

$$\sum_{\alpha} [\phi_i(\alpha) - a_i] \exp\left[-\beta\epsilon(\alpha) - \beta \sum_{j=1}^{L} \pi_j \phi_j(\alpha)\right] = 0 \qquad (1.89)$$

with the correspondence $a(x)\Delta x \to a_i, \phi(x;\alpha)\Delta x \to \phi_i(\alpha)$ and $\pi(x) \to \pi_i$. (Note that both a_i and ϕ_i now have the dimensions of *volume*.) Clearly, the π_i and hence $P(\alpha)$ depend on the aggregation geometry, which in (1.89) is fully accounted for by the a_i.

The $\phi_i(\alpha)$ depend on the nature of the hydrophobic tails. For amphiphiles with simple alkyl tails, $\mathbf{P}$–$(CH_2)_{n-1}$–CH_3, the rotational-isomeric-state (RIS) scheme [129] provides an excellent model ($\mathbf{P}$ denotes the polar head). In this model each of the $n-1$ internal bonds has three possible ("isomeric") states, t, g^+, g^- (t = trans, g = gauche) corresponding to dihedral angles of 0°, +120° and −120°, respectively. The dihedral angle of bond C_k–C_{k+1} is the angle between the planes defined by C_{k-1} C_k C_{k+1}, and C_k C_{k+1} C_{k+2}. All C C C bond angles are fixed (at 112°) and similarly the C–C bond length (at 1.53Å). The energy of a $g^{\pm}$ bond is $\epsilon_g \approx 500$cal/mole relative to $\epsilon_t \equiv 0$. Thus the internal chain energy is $\epsilon(\alpha) = n_g(\alpha)\epsilon_g$, where $n_g(\alpha)$ is the number of $g^{\pm}$ bonds in conformation α. A certain fraction of the 3^{n-1} possible bond sequences, $\{\mathbf{b}\}$, are self-intersecting (non-self-avoiding) and are discarded from the calculation [122–126].

A bond sequence, $\mathbf{b}$, is specified by the $n-1$ rotational isomeric states of the (non-terminal) C–C bonds, e.g., $\mathbf{b} = t, t, \ldots, t$ ("all trans"), $\mathbf{b} = t, t, \ldots, g^-$, etc. Each bond sequence specifies the coordinates of all chain segments relative to any triad of segments, say $\mathbf{P}$–C_1–C_2, but not the overall positional orientation of the chain. We thus characterize an arbitrary conformation α by $\alpha = \mathbf{b}, \Omega, \delta$ with Ω denoting the three Euler angles specifying the overall orientation of the chain, and δ denoting the position of the head group $\mathbf{P}$ within a small interval around the interface. In most calculations so far, all 3^{n-1} bond sequences $\mathbf{b}$ have been generated, and (arbitrarily) sampled with 36 Ω, δ values for each $\mathbf{b}$, thereby obtaining a total of $36 \times 3^{3n-1}\alpha$'s. This number is considerably reduced after discarding those α which violate either the interface inpenetrability or the chain's excluded volume conditions. That is, a chain is restrained from either passing through the interface (into the aqueous region) or intersecting itself. For each α generated, one calculates $\phi_i(\alpha), \epsilon(\alpha) = \epsilon(\mathbf{b})$, and any conformational property of interest, such as bond order parameters or segment distributions in space. The $\phi_i(\alpha)$ are substituted into (1.89) to solve for the π_i. Then, $P(\alpha) = (1/y)\exp[-\beta\epsilon(\alpha) - \beta\sum \pi_i\phi_i(\alpha)]$ is known and can be used to calculate any conformational or thermodynamic property of interest.

The lateral pressure profile in a planar bilayer composed of -$(CH_2)_{11}$–CH_3 chains modeled by the above RIS scheme is shown in Fig. 1.11a. Also shown is the density profile of a free chain $\langle\phi(x)\rangle_f$, as compared to the constant density profile in a compact bilayer, $\langle\phi(x)\rangle = a$. Note that

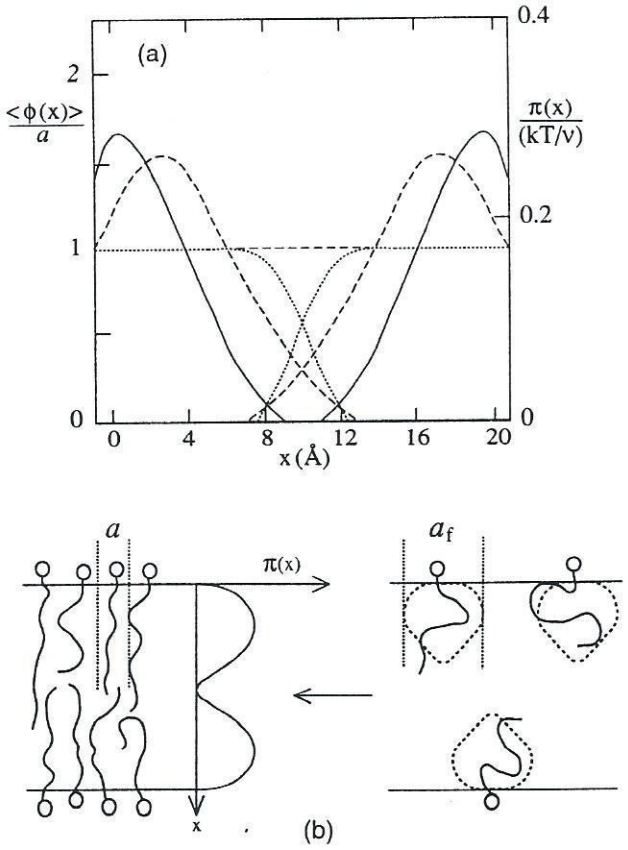

FIGURE 1.11. (a) Normalized density profiles ($\langle\phi(x)\rangle_f/a$, dashed curves) of *free* chains originating from either one of the two interfaces of a planar bilayer composed of twelve-carbon chains, as a function of the distance from one interface. The dotted curves represent the density profiles in each of the two monolayers when the chains are packed with an area per head-group $a = 33\text{Å}^2$. Their sum is the constant monomer density, as described by the horizontal dashed line. The solid lines describe the (normalized) lateral pressure experienced by the chains when packed at the above value of a [124, 125]. (b) Schematic qualitative illustration of the origin of the results shown in (a).

the shape of $\pi(x)$ is qualitatively similar to the chain distortion profile $\langle\phi(x)\rangle_f - a$. Similarly, it has been shown that $\pi(x)$ increases in magnitude as a decreases, consistent with increased chain stretching [124]. A pictorial explanation of these notions is provided in Fig 1.11b.

The singlet *pdf* resulting from the minimization of f_t subject to the *in*equality constraint (1.79) is *also* given by (1.86). As expected, it can be shown that for those values of x for which $\sum P(\alpha)\phi(x,\alpha) = \langle\phi(x)\rangle < a(x)$, the packing constraint is irrelevant, and $\pi(x) \equiv 0$. On the other hand, for those x where $\langle\phi(x)\rangle = a(x)$ we get $\pi(x) > 0$. [Note, however, that since, for all α, $\int \phi(x;\alpha)dx = v$ is the constant chain volume, $P(\alpha)$ and hence also $s_t = -k\sum P(\alpha)\ln P(\alpha)$ remain the same if $\pi(x) \to \pi(x)+$ *constant*. The choice $\pi(x) > 0$ is consistent with the interpretation of π as a pressure. Further support for this choice is given in the alternative derivation of $P(\alpha)$, outlined in section (ii) below.]

Substituting (1.86) into (1.84) and using $\langle\phi(x)\rangle = a(x)$, we get

$$f_t = -kT\ln y - \int \pi(x)a(x)dx \tag{1.90}$$

$$= -kT\ln z \tag{1.91}$$

with the second equality (1.91) serving as the definition of z. Since the integral on the right hand side of (1.90) is a "PV" term, and since f_t is a Helmholtz free energy, the function

$$\mu_t = -kT\ln y \tag{1.92}$$

is the Gibbs potential per chain, i.e., it is the (configurational part of the tail's) chemical potential. Note also that (1.92) is the familiar relationship between the Gibbs free energy (here μ_t) and the isothermal-isobaric partition function (here y). Consistent with these interpretations, it can be shown (see below) that for a planar layer, where $a(x) = a$,

$$\pi_t = \int \pi(x)dx = -\partial f_t/\partial a \tag{1.93}$$

is the total lateral pressure acting on the chains.

Recall that f_t, as given by (1.84), is an approximation to the system's free energy even if $P(\alpha)$ is the exact singlet *pdf*. On the other hand, it is not clear if, and to what extent, Eq. (1.86) for $P(\alpha)$ is an approximation, even though it was derived by the minimization of (1.84). In fact, as will be demonstrated below, conformational properties calculated using (1.86) are in excellent agreement with results from many-molecule computer simulations. An explanation for the high accuracy of (1.86) is provided by an alternative derivation of $P(\alpha)$ which does not invoke explicitly a mean-field approximation. We next sketch briefly this derivation.

(ii) Derivation of $P(\alpha)$ from Z_t

From the definitions (1.75) and (1.77) of $P(\alpha^s)$, and from the assumption (1.82) that $W_t(\alpha^s)$ is dominated by excluded volume interactions, it follows that

$$P(\alpha) = \frac{Z_t(s-1, \tilde{g}(\alpha), T)}{Z_t(s, g, T)} \exp\left[-\beta\epsilon(\alpha)\right] \tag{1.94}$$

Here, $\tilde{g}(\alpha)$ is the geometry of the volume available to the $s-1$ chains surrounding a (central) chain in conformation α. Apart from the Boltzmann factor associated with the self energy $\epsilon(\alpha)$, $Z_t(s-1, \tilde{g}(\alpha), T)$ is the statistical weight of conformation α. The shape of the "hole" prescribed by the α-chain uniquely specifies its area profile $\phi(x;\alpha)$. The geometry, g, of the s-aggregate is characterized by $A(x) = sA(x)$, cf. (1.78). Similarly, the geometry of the $(s-1)$-aggregate, $\tilde{g}(\alpha)$, will be characterized by $A(x) - \phi(x;\alpha)$.

Noting that $\ln Z_t$ is extensive (i.e., of order s), expanding $\ln Z_t(s-1, \tilde{g}(\alpha), T) = \ln Z_t(s-1, \{A(x) - \phi(x;\alpha)\}, T)$ about $A(x)$ and neglecting terms of order $1/s$, we get [120]

$$\begin{aligned} & \ln Z_t(s-1, \{A(x) - \phi(x;\alpha)\}, T) - \ln Z_t(s, \{A(x)\}, T) \\ = \; & -\frac{\partial \ln Z_t}{\partial s} - \int dx \left(\frac{\delta \ln Z_t}{\delta A(x)}\right) \phi(x;\alpha) \\ = \; & \beta\mu_t - \beta \int dx \pi(x) \phi(x;\alpha) \; . \end{aligned} \tag{1.95}$$

Here, $\mu_t = -kT\partial(\ln Z_t/\partial s)_{A(x),T} = (\partial F_t/\partial s)_{A(x),T}$ is the chain's chemical potential, and the functional derivative

$$\pi(x) = kT\frac{\delta \ln Z_t}{\delta A(x)} = -\frac{\delta F_t}{\delta A(x)} = -\frac{\delta f_t}{\delta a(x)} \tag{1.96}$$

is the lateral pressure profile. Substituting (1.95) into (1.94) we regain $P(\alpha)$ as given by (1.86), with a rigorous thermodynamic interpretation of $\pi(x)$ as the lateral pressure and of $\beta\mu_t = -kT \ln y$ as the Gibbs free energy per molecule (cf. (1.92)). Consistent with this interpretation, one can derive additional useful relations, e.g.,

$$\frac{\delta\mu_t}{\delta\pi(x)} = kT\frac{\delta \ln y}{\delta\pi(x)} = a(x) \tag{1.97}$$

which, using (1.87), is recognized as the packing constraint (1.80) in its more explicit form (1.88). Note also that the integral (over x) of (1.96) describes $-\partial f_t/\partial a$ for the case $\partial a(x)/\partial a = 1$, thus leading to (1.93).

The key step in the above derivation is the assumption that $\tilde{g}(\alpha)$ is uniquely specified by $A(x) - \phi(x;\alpha)$. This implies equal statistical weights for all conformations with the same $\{\phi(x;\alpha)\}$ regardless of their exact shape. (The internal energy $\epsilon(\alpha)$ is treated exactly.) A direct way to test

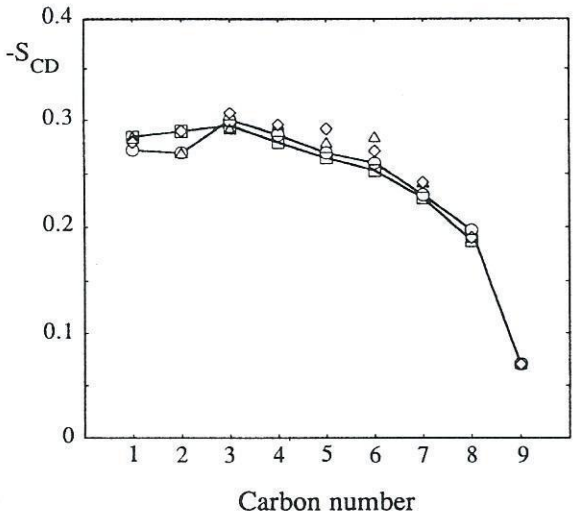

FIGURE 1.12. C–D bond order parameter profiles of C_9 chains packed in a planar bilayer—the area per head-group is $a = 25\text{Å}^2$ [120]. The triangles represent the experimental results of Seelig and Niederberger [131], the squares correspond to the molecular dynamics simulations of van der Ploeg and Berendsen [95] and the diamonds describe the results of Gruen's mean-field theory [116]. The circles describe the results obtained [120] by the mean field theory described in the text.

the accuracy of this prediction and hence of (1.86) is by comparison with computer simulations.

Figure 1.12 shows four C–H orientational bond order parameter profiles, S_k, of -$(CH_2)_8$–CH_3 chains, packed in a planar bilayer with an area per head-group $a = 25.5\text{Å}^2$. The order parameter of C_k–H bond is defined by

$$S_k = \sum_{\alpha} P(\alpha) P_2(\cos\theta_k(\alpha)) \tag{1.98}$$

where $P_2(x) = (3x^2 - 1)/2$ is the second-order Legendre polynomial. $\theta_k(\alpha)$ is the angle between bond C_k–H of a chain in conformation α and the "director", i.e., the normal to the hydrocarbon-water interface. In the limit that all chains are fully stretched (i.e., all-trans) and are normal to the interface, $S_k = -0.5$, since the C–H bonds are then parallel to the interface. On the other hand, for a random distribution of bond orientations, $S_k = 0$. The C–H bond order parameters are simply related to $\tilde{S}_k$, the *skeletal* (C–C bond) order parameters, via $\tilde{S}_k = -2S_k$. $\tilde{S}_k$ is defined as in (1.98) but

with θ_k denoting the angle between the director and the vector connecting carbons C_{k-1} and C_{k+1}.

One of the curves in Fig. 1.12 represents the experimental data of Seelig and Niederberger, obtained from magnetic resonance measurements of the quadrupole splittings of selectively deuterated C–H (i.e., C–D) bonds [131]. These results were accurately reproduced through many-chain molecular dynamics simulations by van der Ploeg and Berendsen [95], who employed realistic intra- and inter-chain interaction potentials. Their results, corresponding to $a = 25.5\text{Å}^2$ are also shown in Fig. 1.12. The value of a is the only input parameter which has been used to calculate the third S_k profile, as outlined above. More explicitly, this value of a was used to calculate $P(a)$ of (1.86) by solving (the discretized) self-consistency equations (1.89) for C_9 chains modeled by the RIS scheme [120]. The agreement between the MD results and the (much simpler) calculations based on (1.86) is obviously excellent. Similar agreement is found with respect to other conformational properties, as well as for average chain energies $\langle\epsilon\rangle$, and entropies $s_t = -k\sum P(a)\ln P(a)$. The fourth S_k profile shown in Fig. 1.12 was obtained by Gruen [116], based on an assumed form for $P(a)$ which is essentially identical to (1.86) (although Gruen's method of calculation was different).

1.3.3.3 Chain conformational characteristics

Using $P(a)$ one can calculate any single chain property of interest. Furthermore, with the aid of mean-field expressions such as (1.84), it is possible to calculate and analyze various thermodynamic functions, for instance, elastic moduli of amphiphilic films, as described in the next section. In this section we briefly discuss some of the basic characteristics of chain packing in planar and curved aggregates.

Some basic qualitative characteristics of chain conformational statistics in micelles and bilayers can be inferred from Fig. 1.11 which illustrates the conformational distortions experienced by free chains upon close-packing among neighboring chains. On the average, a free chain is a "random-coil" with a globular ("turnip-like") shape. The confinement of the chain to one (the hydrophobic) side of the interface includes a certain degree of chain alignment, affecting mainly the first few chain segments connected to the interface. This "residual" ordering is clearly reflected in the order parameter profile of the free -$(CH_2)_{11}$–CH_3 chain anchored to the flat interface of a planar bilayer, as shown in Fig. 1.13. The confining effect of the interface is somewhat more stringent in convex aggregates (such as spherical micelles), implying slightly larger S_k values of the free chains, as confirmed by detailed calculations [121]. Similarly, the conformational free energy, f_t, of a free chain in a micelle is expected to be higher than in a bilayer, because of the greater loss of conformational freedom (see Fig. 1.9). However, in general, the interfacial restrictions on chain conformational freedom are

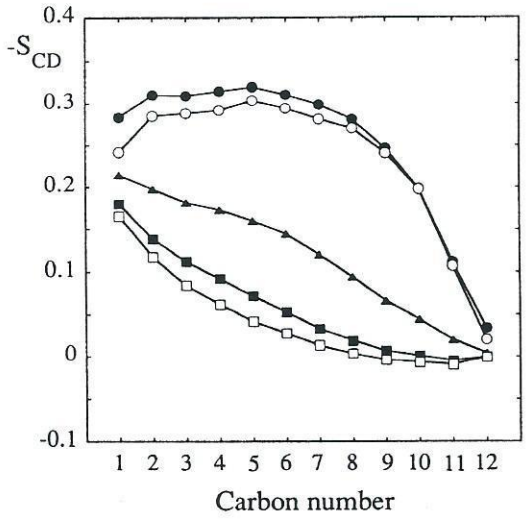

FIGURE 1.13. C–D bond order parameter profiles for C_{12} chains in a planar bilayer. The circles correspond to chains packed with area per head-group $a = 25\text{Å}^2$; the solid circles are for chains with gauche energy $\epsilon_g = 500$ cal/more, whereas the open circles are for "athermal" chains, i.e., $\epsilon_g \equiv 0$. All other data are for $\epsilon_g = 500$ cal/more. The solid triangles represent the results for $a = 32\text{Å}^2$ and the solid squares for $a = 40\text{Å}^2$. The open diamonds are the results for a free chain. (Calculated by D. Hornreich and by I. Szleifer.)

considerably less important than those implied by the packing constraints $\langle \phi(x) \rangle = a(x)$.

As the area per chain in a bilayer decreases, the chains are further squeezed and stretched compared to their free state, resulting in increased values of S_k, cf. Fig. 1.13. Recall from Sec. 1.3.2 that $a = v/R$ in a bilayer, where v is the chain's volume and R is the bilayer's half-thickness. The minimal area per chain, $a_{\min}$, corresponds to fully extended, all-trans, chains so that $a_{\min} = v/l$, where l is the chain length. (For alkyl chains, $a_{\min} \approx 21\text{Å}^2$.) The initial plateau, followed by a rather rapid fall, characterizing S_k in bilayers, can be explained as follows. If the chains were infinitely long we would obviously expect $S_k = \textit{constant}$, since $a(x) = \textit{constant}$. However, since the chains are finite, at some point (say, $\bar{x}$) down the imaginary cylinder implied by $a(x) = a$, they begin to terminate with some distribution of chain ends. Beyond $\bar{x}$, increased conformational freedom (larger effective a) is available to the "dangling ends" of the chains which have not yet terminated, resulting in lower S_k values for the large k [120–122].